Acceleration demands in single-storey RC buildings with flexible diaphragms

ACCELERATION DEMANDS IN SINGLE-STOREY RC BUILDINGS WITH FLEXIBLE DIAPHRAGMS

Sergio Ruggieri [a,*], Vladimir Vukobratović [b]

[a] Department of Civil, Environmental, Land, Building Engineering and Chemistry (DICATECh), Polytechnic University of Bari, Via E. Orabona 4, 70126 Bari, Italy

[b] Faculty of Technical Sciences, University of Novi Sad, Trg Dositeja Obradovića 6, 21102 Novi Sad, Serbia; vladavuk@uns.ac.rs

[*] Correspondence: sergio.ruggieri@poliba.it

ABSTRACT

This paper presents a study on acceleration demands in single-storey reinforced concrete (RC) buildings with flexible diaphragms, expressed through peak floor accelerations (PFAs) and floor response (acceleration) spectra (FRS). Firstly, an extensive parametric study was performed on idealized single-storey buildings for which geometrical parameters were varied for inducing different degrees of diaphragm flexibility. The influence of diaphragm flexibility was taken into account through the commonly used in-plane displacement ratio. To investigate acceleration demands, three sets of Eurocode 8 spectrum-compatible ground motion records were used as input, selected according to three different soil categories. RC buildings were considered as both linear elastic and nonlinear, whereas non-structural components (NSCs) were considered only as linear elastic. In all cases, it was observed that diaphragm flexibility significantly influences PFAs and FRS, which can both increase and decrease compared to buildings with rigid diaphragms. In the case of FRS, a shifting of peaks was observed as well. Despite the very complicated dependence between the diaphragm flexibility and PFAs and FRS, based on the obtained results, simple empirical formulas for the estimation of the ratios between PFAs and FRS in RC buildings with rigid and

flexible diaphragms were proposed. Their accuracy was assessed through a case study example performed on an existing single-storey RC building.

Keywords: Single-Storey RC Buildings, Flexible Diaphragms, Peak Floor Accelerations, Floor Response Spectra, Non-Structural Components.

1. INTRODUCTION

Seismic response of non-structural components (NSCs) sensitive to accelerations caused by earthquakes recently became a hot research topic. This resulted in an obvious improvement of the state-of-knowledge on floor acceleration demands, achieved through new findings from: (1) parametric studies [1,2]; (2) analysis of data from instrumented buildings [3,4]; (3) shake table test results [5,6]; and (4) evaluation of the current code formulas [7,8]. In addition, various approximate procedures for the direct determination of peak floor accelerations (PFAs) and floor response (acceleration) spectra (FRS) were also proposed [9,10,11,12,13]. Of course, the abovementioned studies represent only a part of the recently conducted research, and further insight into the topic can be found in an interesting state-of-the art paper [14], which provides an overview of the most important accomplishments so far, and may serve as a starting point for researchers who are new in this field.

Although significant research efforts have been made in the past to solve various issues related to PFAs and FRS, several challenges still exist. One of the most important issues is the influence of diaphragm flexibility on acceleration demands, which was considered only in few previous studies. In an early study [15], roof accelerations in a single-storey instrumented gymnasium reinforced concrete (RC) building with flexible roof diaphragm were examined. Recordings were obtained during the 1984 Morgan Hill earthquake. It was found that for two considered horizontal directions, accelerations at the roof centre were roughly three times larger than the ones recorded at its edges. When it comes to floor acceleration demands in buildings with flexible diaphragms, some pioneering studies should be mentioned first. Namely, Tena-Colunga [16] and Tena-Colunga and Abrams [17,18] studied increased floor acceleration demands in instrumented buildings by using simple and complex analytical models to define plausible correlations with recorded data. The

same authors showed the spatial variation of floor accelerations and demands in flexible diaphragms by using three-dimensional (3D) finite element models [17,18,19]. After, three existing multi-storey buildings (two unreinforced masonry wall buildings, of which one had RC shear walls, and a timber building with grouted and reinforced masonry shear walls) with flexible diaphragms subjected to the 1989 Loma Prieta earthquake were investigated [20], and their seismic responses were computed and compared with the recorded ones. Also, the responses of their theoretical counterparts with rigid diaphragms were computed for the purpose of comparison. The influence of the diaphragm flexibility on PFAs was presented for two of the buildings, and it was found that its increase can result in increased accelerations. In [21], data recorded from 50 RC shear wall buildings, 50 steel moment frames and 27 steel braced frames were used to examine ASCE 7-10 [22] formulas for the determination of seismic demands on NSCs. Within the study, a special attention was devoted to the diaphragm flexibility influence. Analytical results suggested that PFA amplifications may occur due to the additional deformations induced by the diaphragm flexibility, which can greatly affect the horizontal PFA distribution. It was concluded that the seismic design of NSCs based on average PFAs at a certain floor may not be adequate if a supporting structure exhibits excessive diaphragm deformations. The adequacy of the rigid diaphragm assumption in the FRS computation was investigated by using the seismic response data from the five-storey Costa Mesa City Hall building obtained during the Chino Hills earthquake [23]. It was stated that the diaphragm flexibility, even at relatively low frequencies, may play an important role in the determination of accurate FRS for the NSC checking. In a study that considered the role of diaphragm flexibility in the seismic analysis of existing masonry structures [24], it was found that with increasing diaphragm flexibility there is an increase in PFA demands, for both elastic and inelastic responses. In the above-mentioned study [3], in which 59 instrumented buildings were examined, the effects of diaphragm flexibility were considered in detail. It was observed that in many of the buildings they produced inconsistencies in FRS. The study showed that in buildings with perimeter lateral force-resisting systems diaphragm flexibility can increase PFAs at floor mid-spans with respect to edges, whereas the opposite trend was noticed in buildings with core lateral force-resisting systems.

In order to properly present the results of this study, it is necessary to provide an insight into the main terms related to diaphragm flexibility. It is well-known the main role of a floor system is to distribute loads acting on a horizontal system to the underlying elements in accordance with the stiffness of vertical elements (e.g., columns, walls). The hypothesis is valid only if a floor is infinitely rigid in its own plane, but it may not always be on the safe side. Generally, within the requirements of the main international building codes, qualitative (e.g., Eurocode 8 [25]) and quantitative criteria (e.g., International Building Code, IBC [26]) are assumed to define the in-plane diaphragm flexibility. The main representative parameter is usually the in-plane displacement ratio, λ, defined as the ratio between maximum and minimum displacements under horizontal static loads. Looking at the studies on the influence of diaphragm flexibility, the early most significant contributions were provided in [27], in which a sensitivity analysis on several RC models was performed and the most influencing parameters on flexibility were defined (e.g., presence of lateral shear walls). An error given by the rigid diaphragm assumption in flexible systems was also quantified, by means of a geometrical factor, termed the rigidity factor, R_i, defined as the ratio between the in-plane stiffness and the lateral stiffness. In [28], authors performed an interesting study on the diaphragm flexibility in which the influences of different floor plans (e.g., rectangular, L-shaped, U-shaped, T-shaped) and lateral resisting systems (e.g., frames and walls) were investigated, resulting in a simple formula for the realistic evaluation of the diaphragm flexibility. In [29], the effects of inelastic flexible diaphragms were investigated on a regular RC building consisted of internal moment-frames and external shear walls. It was shown that the rigid diaphragm assumption provided an incorrect shear distribution among vertical elements, and non-conservative analysis results were obtained for internal moment-frames given by an increment of strength and ductility demands. Several other works can be considered for highlighting the influence of diaphragm flexibility on structures. For example, the variation of modal parameters among the same buildings with and without the diaphragm flexibility assumptions was demonstrated in [28,30,31,32]. The fairly popular modal shifting effect was defined, which can provide an inversion of the fundamental vibration modes order. In the recent works by Tena-Colunga and associates, new information about the flexibility were provided, accounting for the effects of slab thickness [33] and openings in vertical elements [34]. In

addition, Tena-Colunga provided a vision about the topic with regard to the observations made on buildings damaged during the 2017 Mexico City earthquake, in which diaphragm flexibility was considered as an additional irregularity source [35]. In the end, for the sake of brevity, a comprehensive state-of-the-art about the topic was reported in [36,37], in which the main parameters influencing the diaphragm flexibility were highlighted, especially in the case of RC buildings. These parameters are: (a) the typology of a slab and, in the case of a ribbed one, the orientation of joists with respect to the horizontal action direction; (b) the number of storeys and the building height; (c) the ratio between the external sides of a building, also named the in-plane shape ratio; (d) the presence of in-plane irregularities (e.g., large openings, in-plane set-backs); (e) relative stiffness among horizontal and vertical elements, accounting for the dimensions of the latter.

The main goal of this paper is to provide a contribution to the state-of-knowledge on PFAs and FRS, by taking into account the influence of diaphragm flexibility in more detail than it was previously done. An extensive parametric study was conducted on a large number of idealized single-storey RC buildings, and an existing building was analysed to check the findings in practical terms. Namely, PFAs and FRS on some strategic points on the floor were determined and elaborated, after performing both linear and nonlinear time history analyses, and a comparison between models with rigid and flexible diaphragms was conducted. The observations on the behaviour were used to quantify the differences between the two assumptions, by providing practical proposals to estimate the PFA and FRS differences ("errors"). The variation of geometrical parameters in the idealized models (see Section 2.1) was not used for carrying out a sensitivity analysis, but to create an extensive sample of case studies able to simulate a large range of possibilities where diaphragm flexibility can occur. The paper is organized as follows: properties of considered idealized buildings, modelling assumptions and seismic input are provided in Section 2; the PFAs and FRS are presented and discussed in Sections 3 and 4, respectively; the case study example is provided in Section 5; and the main conclusions are given in Section 6.

2. CONSIDERED BUILDINGS AND SEISMIC INPUT

2.1 Buildings, modelling and diaphragm flexibility

To investigate the influence of the diaphragm flexibility assumption on PFAs and FRS, a set of idealized regular RC existing buildings were analysed. In this phase, the research design aimed towards emphasizing the flexibility effect, by using only single-storey buildings. As a matter of fact, and as stated in [37], diaphragm flexibility is too evident in single-storey buildings, considering that the weight of upper floors in multi-storeys buildings leads to a stabilising effect. The buildings investigated herein were moment-frame structures, regular in-plane, and constituted of rectangular floor areas. Their numerical models were 3D with the two main horizontal directions denoted as *X* and *Y*. Therefore, in order to perform the parametric analysis, the set of buildings was simulated by varying several geometrical parameters, as shown in Table 1. In particular, the varied geometrical parameters were: (1) the bay lengths in *X* and *Y* directions, which influence the in-plane floor area and the total length of buildings in both main horizontal directions; (2) the number of bays in *X* and *Y* directions, which outlined the in-plane shape of the buildings and defined the in-plane shape ratio (herein evaluated as the ratio between the lengths in *Y* and *X* directions); (3) the size of external columns in *Y* direction, which allowed to simulate the diaphragm flexibility with a parabola-like shape along the *Y* direction (also defined as an arch effect in [37]). The latter assumption was combined with a cross-sectional size of internal columns fixed to 30 x 30 cm (the number of internal columns depended on the number of bays in both main directions), and the size of external rectangular columns in *X* direction was fixed to 30 cm. Following an idea reported in [38] to investigate bi-directional pushover on increasingly irregular models, the variation of the size of external columns in *Y* direction simulates several occurrences that provoke diaphragm flexibility effects in existing buildings: the presence of external shear walls towards internal thin columns; retrofit solutions providing the regularization of the dynamic behaviour of buildings through more stiff vertical elements (e.g., RC jacketing); the presence of strong external masonry infills, as defined in [39]. Still, the accounted combinations of varied geometrical parameters were selected in order to avoid that the length of the building side in *X* direction is greater than the one in *Y* direction, to have an even number of bays in *X* direction, and to prevent unrealistic situations, such as extremely high in-plane shape ratio (e.g., the combination with 1 bay in *Y* direction and 12 bays in *X* direction was avoided).

Based on the above, the total number of generated single-storey buildings was 112 (from 192 possible combinations). For each building, 4 numerical models were created by using OpenSees [40], and as reported in Figure 1: (a) a linear elastic model with a rigid diaphragm; (b) a linear elastic model with a flexible diaphragm; (c) a nonlinear model with a rigid diaphragm; (d) a nonlinear model with a flexible diaphragm. To simulate the rigid diaphragm an internal constraint was used, while a strut model was employed to simulate the diaphragm flexibility. In particular, two planar cross braces (simulated through *corotationalTruss* elements) were inserted at floor areas, evaluated trough an equivalence with the in-plane slab stiffness, as employed in [37]. In the case of linear elastic structures, beams and columns were modelled with *elasticBeamColumn* elements, while in nonlinear models the structural elements were simulated by using *beamWithHinges* elements. The latter allowed to simulate mechanical nonlinearities through a lumped plasticity approach, where each plastic hinge was assembled through *Pinching4* material. Plastic hinges accounted for deterioration, as proposed in [41]. Constitutive laws of plastic hinges were defined in terms of moment-rotation, as defined in Eurocode 8 [25], only accounting for bending mechanisms (for columns, a constant axial stress was considered, obtained from the seismic combination of loads). In column hinges the bi-directional behaviour of sections was taken into account through the *sectionAggregator* option, while beam hinges were defined as mono-directional. In all models, columns were fixed to the ground by using external restraints, while brittle mechanisms and node failures were neglected in order to avoid adding of other variables to the investigated problem.

When it comes to loads, a typical value for residential buildings was used, so dead loads were assumed to be equal to 5.5 kN/m^2 and live loads were assumed to be equal to 2 kN/m^2. Hence, by employing the seismic combination of loads by means of the quasi-permanent combination coefficient for live loads, the total load amounted to about 6.1 kN/m^2. From the total weight computation, nodal masses were determined and properly distributed to floor nodes. In the end, some other parameters were fixed as constant for all models. In fact, the simulated slab typology was assumed as typical for the Mediterranean area, as well as RC ribbed slabs oriented in *Y* direction, made by constant joists having height equal to 20 cm and width equal to 10 cm, spacing between adjacent joists equal to 50 cm, a thickness of the top concrete slab equal to 4 cm, and

hollow clay blocks among joists. Concrete with the compressive strength of 25 MPa and an elastic modulus of 31.5 GPa was considered, while for steel reinforcement a tensile strength of 450 MPa and an elastic modulus of 210 GPA were taken into account.

Table 1 – Varied geometrical parameters of the considered idealized buildings assumed for the parametric analysis

Geometrical parameters	Assumed values
Bay length in *X* direction (m)	(5, 6)
Bay length in *Y* direction (m)	(3, 4)
Number of bays in *X* direction	(2, 4, 8, 12)
Number of bays in *Y* direction	(1, 2, 3)
Size of external columns in *Y* direction (cm)	(50, 100, 150, 200)

Once numerical models were established, the linear elastic models were firstly used to evaluate the effects of diaphragm flexibility on PFAs and FRS, while nonlinear models were subsequently considered for accounting the nonlinearities. Still, the analyses (linear static and linear/nonlinear dynamic, as later reported), were performed only in *Y* direction, to examine the in-plane flexibility. The latter was investigated from the results obtained at several selected points of the models, i.e., the external point P_{EXT}, and the central point P_{CEN} (see Figure 1). Obviously, in the case of rigid diaphragm and by assuming the left P_{EXT} as the reference point, the obtained results in the rightmost point of the slab are the same, since as there are no torsion effects.

The first analytical operation on numerical models was the quantification of the diaphragm flexibility by means of the definition of λ. To this scope, all linear elastic models with flexible diaphragms were subjected to horizontal static forces applied at all nodes of the first storey, by assuming a unitary resultant force for each numerical model. The values of λ were evaluated for all models as the ratio between the horizontal displacements recorded at P_{CEN} and P_{EXT}. The obtained results showed that the less deformable models led to the value of λ close to 1, e.g., for the structures having minimum size of external columns in *Y* direction

(50 cm) and in-plane shape ratio (about 2). The most flexible models had λ values higher than 3, especially in the cases of structures having maximum size of external columns in Y direction (200 cm) and in-plane shape ratio (about 4). Based on [26], the limit of λ for classifying models as flexible is equal to 2 but, in this analysis, also models with lower values were considered for evaluating the effects on PFAs and FRSs (for λ ranging from 1 and 2, models are usually considered as stiff, as well as being between rigid and flexible).

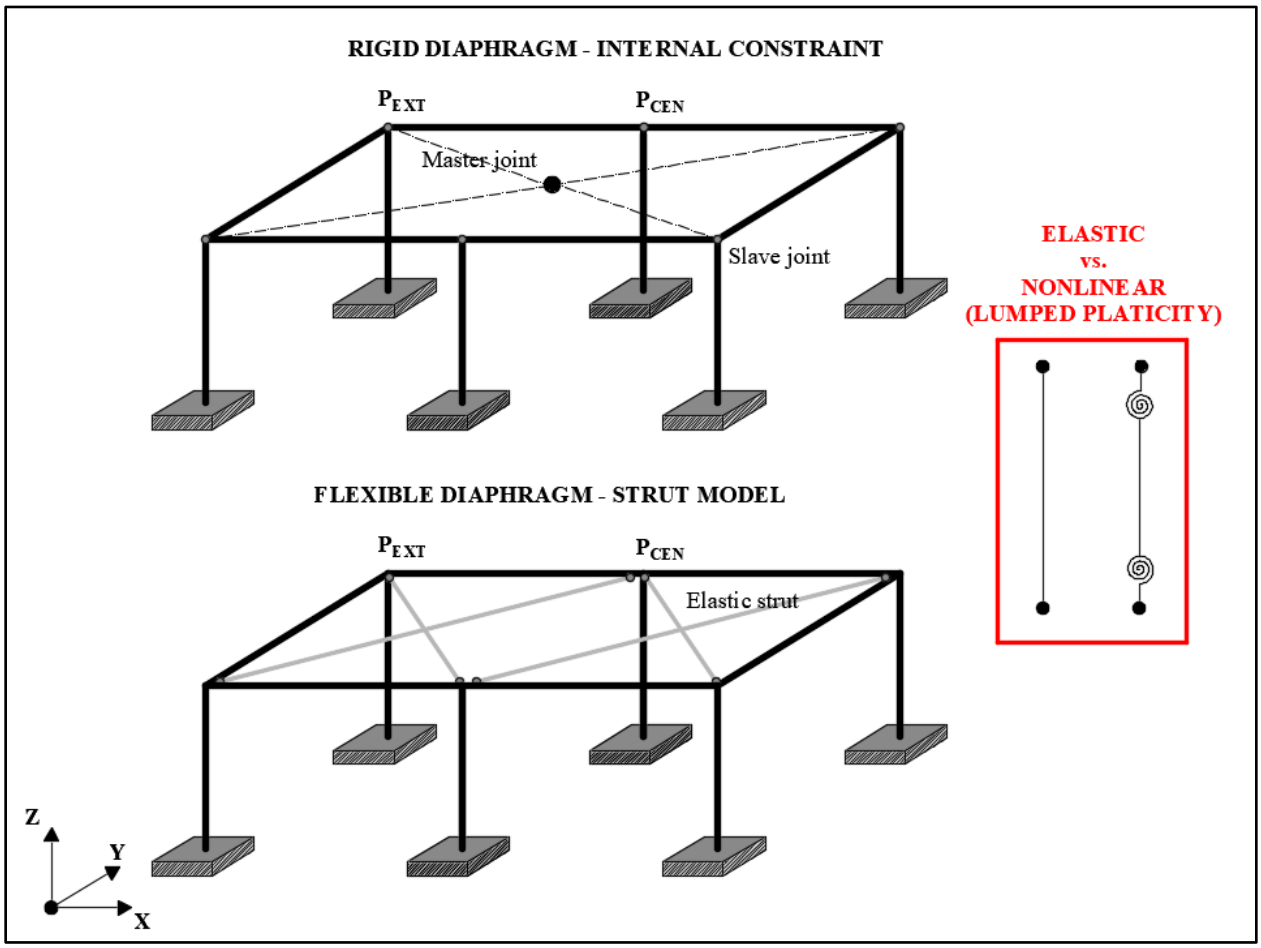

Figure 1 – Modelling approaches for 112 idealized buildings: rigid vs. flexible diaphragm and linear elastic vs. lumped plasticity (with rotational springs) structural elements. Indication of the external and central points, P_{EXT} and P_{CEN}, respectively.

Hence, it is worth noting that the real advantage of λ, which is the recurring parameter throughout this paper, is the fact that it represents the most practical way to quantify the diaphragm flexibility. Finally, eigenvalue analyses were performed on numerical models and the values of vibration periods (with regard

to the *Y* direction, which is the direction of interest) of rigid diaphragm models ranged from 0.05 to 0.42 s and periods of flexible diaphragm models ranged from 0.06 to 0.44 s, with a maximum difference between the two model types of about 0.08 s.

2.2 Seismic input and its application

The applied seismic input consisted of 3 three sets having 11 ground motion records each, selected from the European-Strong-Motion-Database [42] and in accordance with 3 different soil categories: A, B and C (according to [25]). In particular, for each soil category, the selection was arbitrarily made according to previous studies (e.g., [43,44]), referring to a specific target spectrum and accounting for different amplification conditions that can occur in a low-medium period range since it is of interest for the studied structures. As a basis for the ground motion selection, Eurocode 8 target spectra were used. Accordingly, there is no strict code-defined rule regarding the earthquake nature. In other words, as it can be seen from Figure 2, some records are well-below and well-above the target spectra. The authors believe that in this way a broader range of possible earthquakes is taken into account, compared to the option in which scaling of records is performed in order to find a close match to the target spectrum. The record-scaling option was also omitted due to the fact that code-based spectra are used both for analysis and design, and the latter is beyond the scope of the paper. In this way, the effects of the diaphragm flexibility were also assessed for three different levels of the seismic input, which could represent an important variable in the problem under investigation. For the case at hand, the record selection was performed in agreement with Eurocode 8 provisions, and limit differences between mean and target spectra amounted to +30% and –10%. The fitting was performed between 0.05 and 1.0 s, and the latter value is approximately twice larger than the maximum fundamental period of vibration of the structures under investigation. Elastic ground motion spectra for all individual records, their mean and target spectra, all for 5% damping, are shown in Figure 2 (*T* denotes the period, *g* is the acceleration of gravity). Information about the applied ground motions is provided in the Appendix.

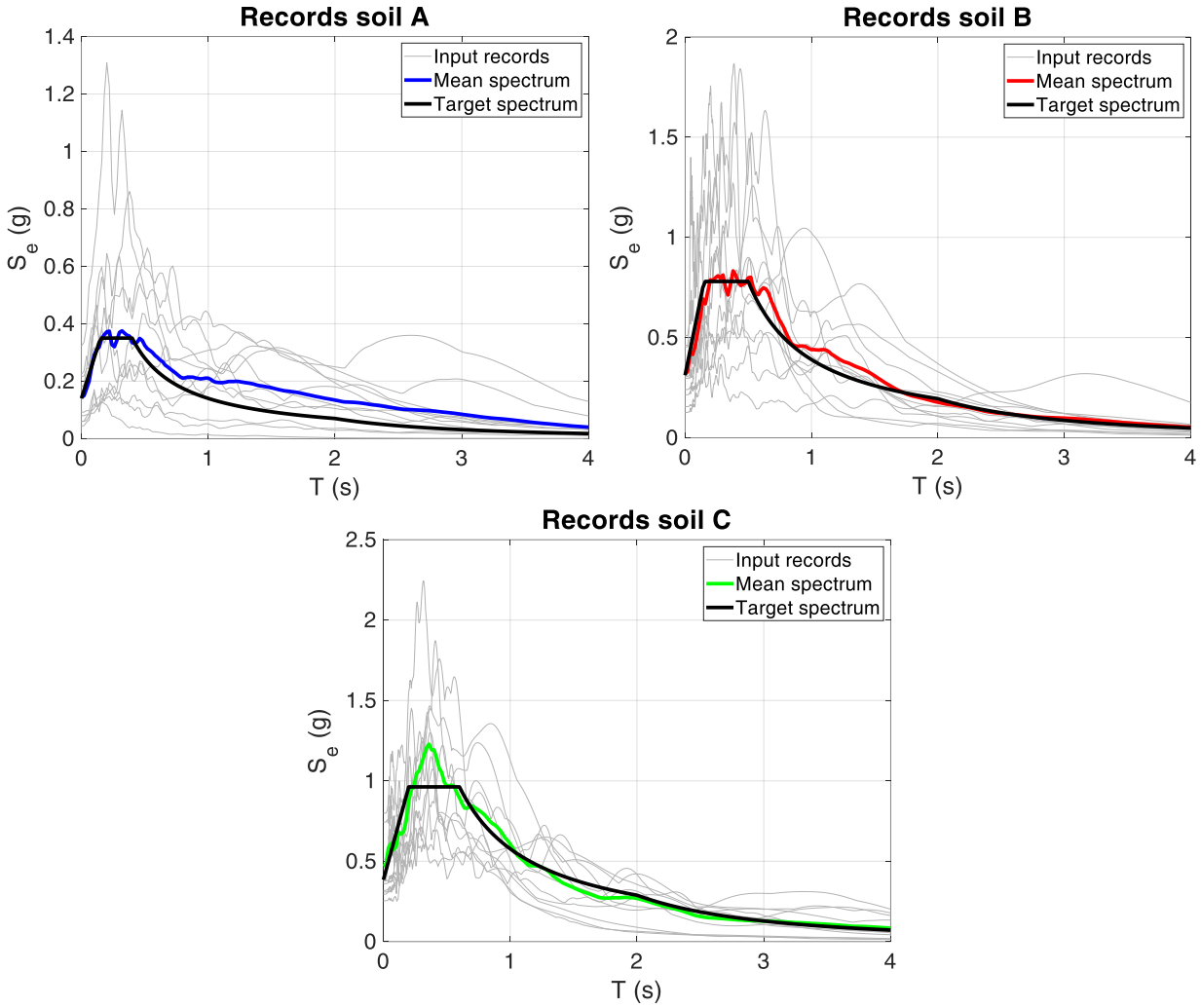

Figure 2 - Elastic acceleration spectra (S_e) of individual records from the considered sets, their mean elastic spectra, and the target Eurocode 8 spectra (all for 5% damping).

For the soil A set (blue line) the mean value of peak ground acceleration (PGA) is equal to 0.15 g, for the soil B set (red line) the mean PGA is equal to 0.32 g, whereas for the soil C set (green line) the mean PGA is 0.43 g. When it comes to the target spectra shown in Figure 2, the PGA values for sets corresponding to soils A, B and C are equal to 0.15, 0.31 and 0.39 g, respectively. All models considered in this study were excited by applying one record at a time in *Y* direction, and all obtained results are shown below.

2.3 Assessment of the floor modelling strategy and of the monitored points

Despite the provided definition of the floor modelling strategy and the selected seismic input for the analyses to run and the points to monitor, in the authors' opinion a specific deepening must be devoted to these delicate aspects. First, the proposal for the modelling of flexible floors relies on the most practical method employed in 3D numerical models, as well as on the use of two elastic planar cross braces, as done in [37]. This method was well defined in [45], where an equivalence between the in-plane stiffness of the slab (K_s) and the one of the braces (K_b) was achieved through the equation

$$K_s = \frac{1}{\frac{L'^3}{12 \cdot J \cdot E_s} + \frac{L'}{A_s \cdot G_s}} = K_b = \frac{E_b \cdot A_b}{L_b} \quad (1)$$

where L' is the floor dimension orthogonal to the horizontal action, J is the inertia moment of the slab section, E_s and G_s are the elastic and shear moduli of the slab material, respectively, E_b is the elastic modulus of braces, A_s is the shear area of the slab, and A_b and L_b are the area and length of braces, respectively. Then, the equivalence in Eq. 1 allows the determination of A_b. A greater degree of detail can be achieved by employing an elastic shell (e.g., [46]) that, when talking about a typology of ribbed slab as the one used in this paper, must necessarily be orthotropic. In the scientific literature some methodologies based on parametric analyses and numerical simulations [36, 47] are proposed, where the accuracy of the results depends on the provided thickness, the elastic moduli in both main directions, and the mesh of the applied numerical element. Very few works proposed a nonlinear floor modelling, considering that the main goal to simulate floor flexibility resides in a more realistic prediction of the force distribution in structural elements. For example, in [30] authors proposed a floor modelling through bilinear springs with stiffness-degrading hysteretic properties. Nevertheless, the real absence of experimental investigations on the floor flexibility of lightening ribbed slabs does not provide sufficient information to perform a real nonlinear slab simulation. Recently, a valuable attempt in this direction was proposed by [48], where authors identified 3 possible failure mechanisms of ribbed slabs, and they experimentally investigated the most likely one. As a matter of fact, for simulating the slab failure under arch loading and deformation, authors performed shear

experimental tests on some modular sub-assembly specimens, made by a single hallow clay block and a concrete joist. Afterwards, a refined model was calibrated where a homogeneous equivalent inelastic material was defined. The material was assigned to a shell element, for which nonlinear properties were assumed as elastic-perfectly plastic in compression and elastic with softening after yielding in tension.

Besides the floor modelling techniques, another important aspect is related to the selection of monitoring points. For the case at hand, P_{CEN} and P_{EXT} were selected, but also the midspan point (P_{MID}) deserves attention, considering the fact that the acceleration amplifications on the floor can act on some assets contained in the buildings, which are not located on the sides (monitored points), but around P_{MID}. Still, as shown in some studies (e.g., [46]), the influence of earthquake actions on structures can be investigated by observing the effects at the midspan.

For the scope of this paper, before proceeding with the analysis campaign, it is necessary to assess both aspects, ensuring that the assumptions reported in Section 2.1 are accurate enough. Thus, to cover the extreme scenarios in terms of flexibility, from the generated numerical samples, 3 models were selected. These are the models with lower (bay lengths of 5 and 4 m in *X* and *Y* directions (respectively), number of bays in *X* and *Y* directions equal to 4 and 2 (respectively), cross-sectional size of external columns of 30 x 50 cm, λ equal to 1.10) and higher values of λ (bay lengths of 6 and 3 m in *X* and *Y* directions (respectively), number of bays in *X* and *Y* directions equal to 12 and 3 (respectively), cross-sectional size of external columns of 30 x 200 cm, λ equal to 3.40) and the model having the value of λ closest to 2, according to the limit proposed by [26] (bay lengths of 5 and 3 m in *X* and *Y* directions (respectively), number of bays in *X* and *Y* directions equal to 8 and 2 (respectively), cross-sectional size of external columns of 30 x 100 cm, λ equal to 2.02). For the 3 models, 3 modelling strategies of the floor were applied: (1) elastic cross braces, according to Eq. 1; (2) elastic orthotropic shell with equivalent thickness, according to [36]; (3) nonlinear isotropic shell with equivalent material, according to [48]. For the 9 models, nonlinear time history analyses were performed for all ground motion records discussed in Section 2.2. The nonlinear modelling of structural elements follows the concepts reported in Section 2.1. All the information about the floor modelling is reported in Table 2, where the models with higher and lower flexibility, as well as the model

having λ closest to 2, are indicated as $M_{\lambda MIN}$, $M_{\lambda MAX}$, $M_{\lambda LIM}$. Thickness of the elastic cross braces indicates the section side of each brace assumed as square, while thickness of the elastic shell varies according to the structural elements' size. Elastic modulus of nonlinear shell was estimated by balancing the effective geometry of the two materials constituting the slab and their elastic moduli.

Table 2 – Floor modelling properties for $M_{\lambda MIN}$, $M_{\lambda MAX}$, $M_{\lambda LIM}$.

Model	Floor modelling typology	Thickness (cm)	Elastic modulus (GPa)	Compressive concrete strength (MPa)
$M_{\lambda MIN}$	Elastic cross braces	28.7	31.5	/
	Elastic shell [36]	4.5 – 4.7	31.5	/
	Nonlinear shell [48]	25.0	20.5	8.00
$M_{\lambda MAX}$	Elastic cross braces	20.5	31.5	/
	Elastic shell [36]	2.0 – 4.7	31.5	/
	Nonlinear shell [48]	25.0	20.5	8.00
$M_{\lambda LIM}$	Elastic cross braces	22.2	31.5	/
	Elastic shell [36]	4.0 – 4.7	31.5	/
	Nonlinear shell [48]	25.0	20.5	8.00

With regard to the different floor modelling assumptions, some results are provided in Figure 3, where 3 graphs are presented, each one reporting time histories (with ground motion records arbitrarily selected within the 3 sets) for a specific model and the 3 types of floor modelling, monitoring the point at higher flexibility, P_{CEN} (quasi-identical results are obtained for P_{EXT}). As shown in Figure 3, some differences are obtained by varying the floor modelling assumptions, but looking at the values of PFAs, the values do not substantial differ. In order to trace a general trend, the results from models with nonlinear shell are lower than the elastic ones, with peak variation of around 10% in $M_{\lambda MAX}$ (lower differences are overall obtained for $M_{\lambda LIM}$ and $M_{\lambda MIN}$). Still, negligible differences are recorded between the elastic models. In the end, a floor modelling with elastic elements provides close results to the ones obtained from the nonlinear

approach, with some main advantages: (i) a sensible reduction of the analysis time; (ii) a slight beneficial conservatism; (iii) an evident practical application, especially in favour of the elastic braces, can makes the floor modelling accessible to all engineers. Given the above advantages, the analysis campaign will be performed by using the simplest approach among the discussed ones.

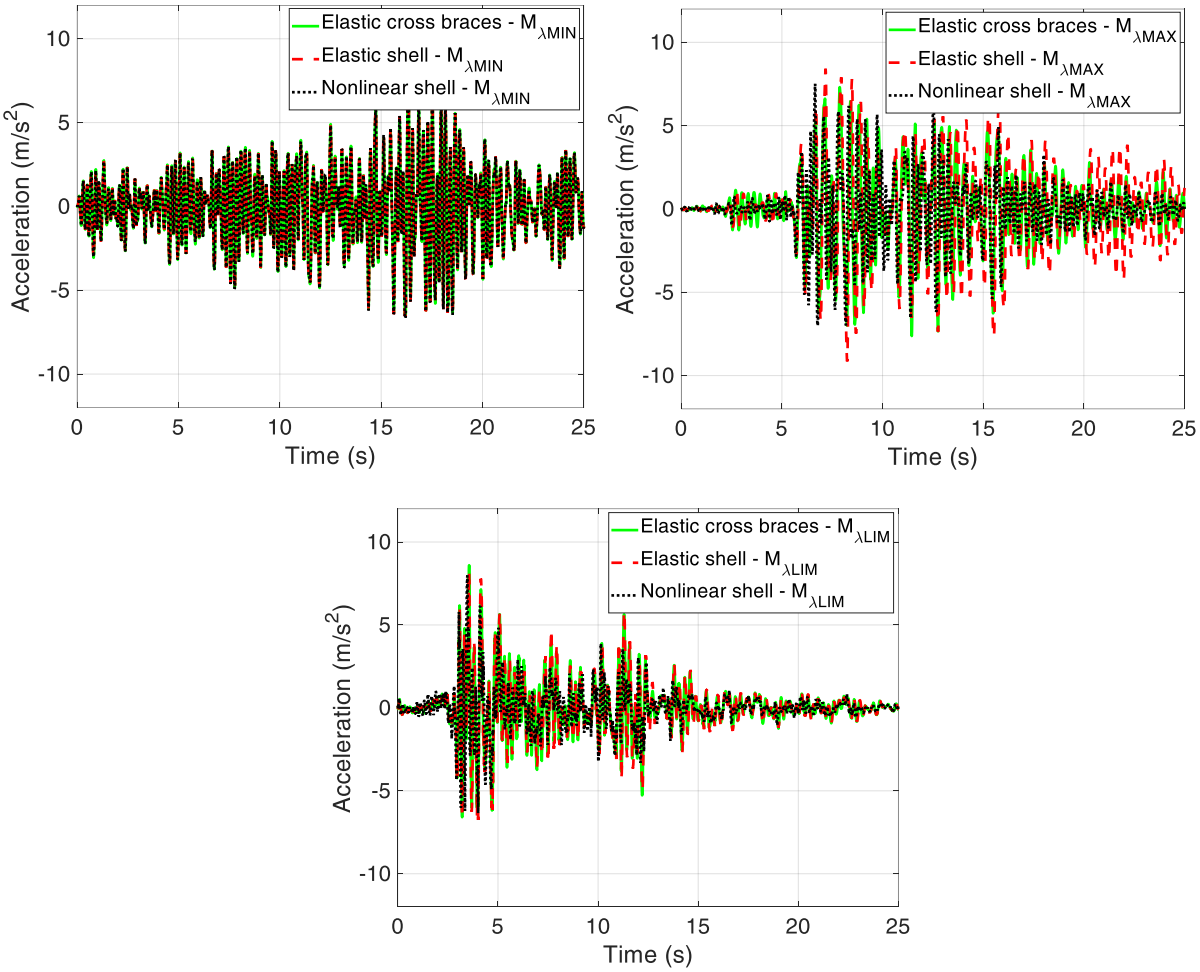

Figure 3 – Absolute acceleration time histories for $M_{\lambda MIN}$, $M_{\lambda MAX}$, $M_{\lambda LIM}$, accounting for different floor modelling strategies and using different input.

The last control to perform is about the difference among the accelerations recorded in the points selected in Section 2.1 (P_{EXT} and P_{CEN}) and the midspan point (P_{MID}). With this regard, the results of this first analysis campaign are provided in Figure 4, where for $M_{\lambda MAX}$ (results on other models are not shown only for the sake of brevity) time histories for one ground motion record are shown for all floor modelling approaches and for the 3 selected points. The responses suggest that the PFAs recorded at P_{CEN} are always greater than

the ones obtained at P_{MID} and at P_{EXT}. The obtained results suggest that the higher accelerations are obtained at the points related to higher flexibility, which will be accurately faced later. Nevertheless, this is not true in general, considering the nature of the numerical samples (one-storey buildings within a short range of periods). Thus, for the scope of this paper, the analysis campaign can be limited to the PFAs at P_{EXT} and P_{CEN}.

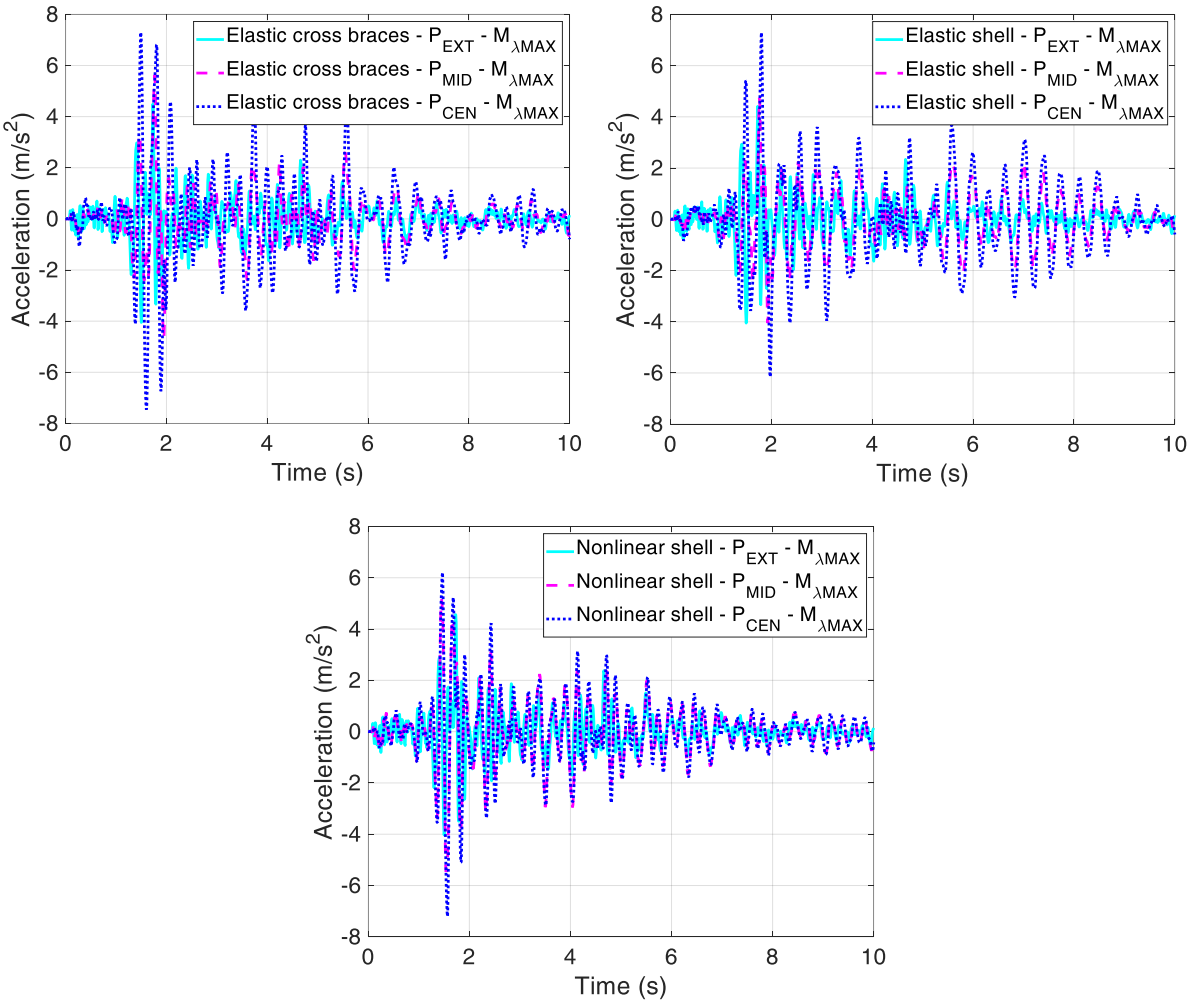

Figure 4 – Absolute acceleration time histories for $M_{\lambda MAX}$, accounting for different floor modelling strategies and monitoring at P_{EXT}, P_{CEN} and P_{MID}.

3. PEAK FLOOR ACCELERATIONS

3.1 Estimation of PFA ratios between rigid and flexible diaphragm buildings

Once λ values were determined and the floor modelling assumptions and the points to monitor were assessed, time history analyses were performed on the linear elastic models, by applying one record at a time in Y direction, which led to a total of 7392 analyses (112 models, 2 floor modelling assumptions, and 11 accelerograms for 3 soil categories). Afterwards, floor acceleration time histories were recorded at P_{CEN} and P_{EXT}, for both rigid and flexible diaphragm models, and subsequently PFAs were extracted from both monitored points. In Figure 5 two examples of response histories are shown on the model having bay lengths of 5 and 4 m in X and Y directions, respectively, the number of bays in X and Y directions equal to 4 and 1, respectively, with cross-sectional size of external columns of 30 x 150 cm (in X and Y directions, respectively) and the value of λ equal to 1.80. The results are reported for arbitrarily selected 2 (out of 11) applied ground motion records for soil B.

Firstly, for rigid models, absolute floor accelerations are completely the same at P_{CEN} and P_{EXT}, which is expected by considering the regularity of numerical models. By looking at the flexible models, the recordings at P_{CEN} and P_{EXT} deviated from their counterparts obtained for the rigid models, showing an increase in floor acceleration for P_{CEN}, and a decrease in floor acceleration for P_{EXT}. Obviously, the different flexibility of the models provided a different swing phase for the monitored points. Nevertheless, the different amplitude between analogous models is of greatest interest, which occurred in all investigated cases. The deviation of the acceleration could be quantified along the entire response history, but from a practical point of view it is more important to quantify variations in terms of PFAs. Still, as in the case study shown in Figure 5, also for flexible models having values of λ lower than 2, the variations in terms of absolute acceleration can be considered as consistent.

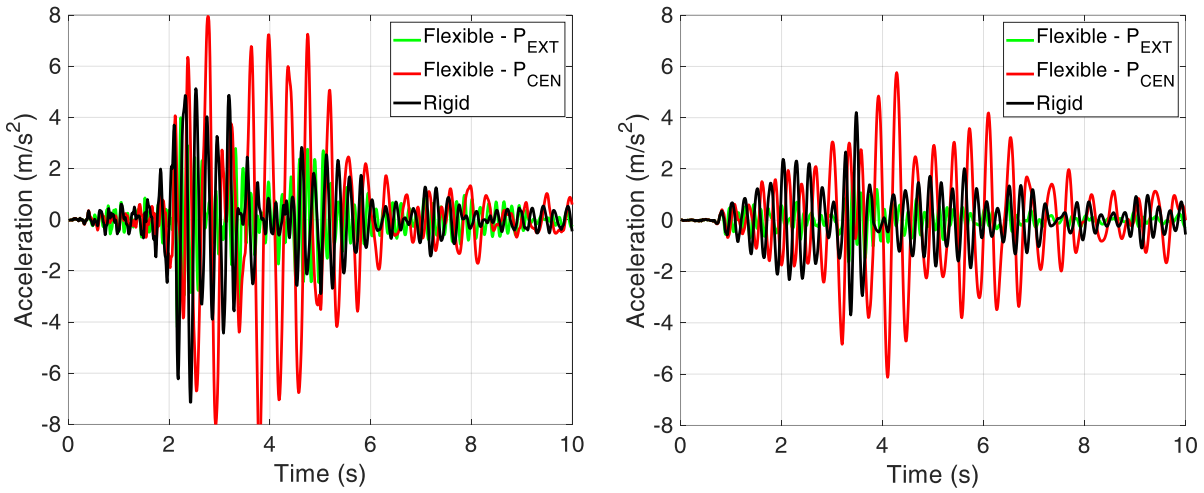

Figure 5 – Absolute acceleration time histories for two arbitrarily selected ground motion records (soil B), for rigid and flexible (λ = 1.8) models.

According to the above concept, all values of PFAs are shown in Figure 6, where three graphs are presented for all considered soil categories. In particular, in each graph it is illustrated the relation between the PFAs recorded at P_{CEN} of rigid models vs. the PFAs recorded at P_{EXT} (green points) and at P_{CEN} (red points) of flexible models. The PFAs were normalized to the values of mean spectra PGAs reported in Section 2.2, according to corresponding soil categories, in order to show results in non-dimensional way. For the sake of clarity, PFAs for rigid models are indicated as PFA_R, while the PFAs on flexible models are denoted as PFA_{F+} and PFA_{F-}, with regard to P_{CEN} and P_{EXT}, respectively. In Figure 6, PFA_{F+} and PFA_{F-} are plotted on the same axis and then the axis caption is indicated as $PFA_{F+/-}$.

Looking at the analyses results, it can be observed that for a given value of PFA_R, the value of PFA_{F+} is greater than PFA_{F-}. This trend is observed for all models and the differences between PFA_{F+} and PFA_{F-} increase for higher values of PFAs. In general, going from the lower to the higher values of PFAs, a regular increasing dispersion can be denoted, even though in some few cases the values of PFA_{F+} are out of the general trend (see for example soil C, for values of PFA_R/mean PGA lower than 5). This can be due to a number of reasons, such as the type of ground motion record, the type of building and their interaction.

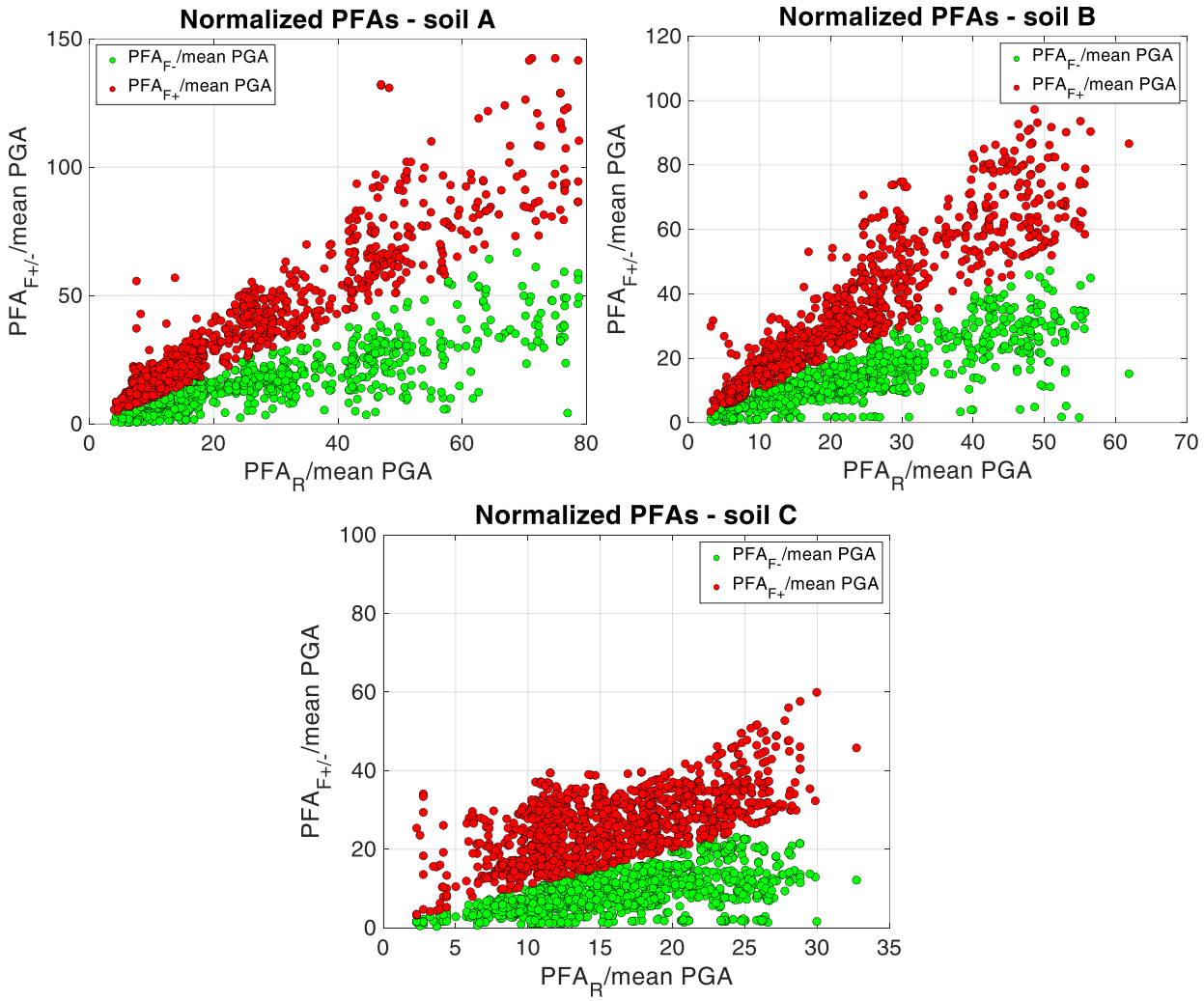

Figure 6 – Normalized PFAs for rigid and flexible linear elastic models, for each soil category.

Nonetheless, although an obvious pattern between greed and red points is shown in Figure 6, the aim of this paper is to provide a way to relate the observed effect on the PFA variation to the effective diaphragm flexibility of the models, which can be quantified through λ. In addition, to estimate the PFA variation between the rigid and flexible models, the most popular approach is to evaluate the ratio between PFAs at P_{CEN} in them (PFA_{F+} vs. PFA_R) and the ratio between PFAs at P_{EXT} (PFA_{F-} vs. PFA_R). To define the above ratios, the PFA variation from rigid to flexible models was estimated as

$$R_{PFA,F+} = \frac{PFA_R}{PFA_{F+}}; R_{PFA,F-} = \frac{PFA_{F-}}{PFA_R};\ for\ soils\ A, B, C \tag{2}$$

where $R_{PFA,F+}$ is the ratio between the PFAs at P_{CEN} in rigid and flexible models, while $R_{PFA,F-}$ is the ratio between the PFAs at P_{EXT} in flexible and rigid models. It is worth noting that the ratios in Eq. 1 were imposed in order to be between 0 and 1, instead of to be always referred to the PFAs in rigid models. This allows to allocate the values of the above ratios in a predefined range, avoiding to have higher dispersion of data in the higher range of values.

Adopting this approach, the values of $R_{PFA,F+}$ and $R_{PFA,F-}$ can be correlated with the values of λ. To this scope, and considering that a value of λ correspond to 11 values of PFAs for each model and each soil type, a mean approach is employed, transforming terms of Eq.1 in

$$R_{MPFA,F+} = \frac{\frac{\sum_{i=1}^{N} PFA_{R,i}}{N}}{\frac{\sum_{i=1}^{N} PFA_{F+,i}}{N}}; R_{MPFA,F-} = \frac{\frac{\sum_{i=1}^{N} PFA_{F-,i}}{N}}{\frac{\sum_{i=1}^{N} PFA_{R,i}}{N}};\ for\ soils\ A, B, C \tag{3}$$

where N indicates the number of records run on each numerical model and $R_{MPFA,F+}$ and $R_{MPFA,F-}$ are the ratios between the mean PFAs at P_{CEN} in rigid and flexible models and the ratio between the mean PFAs at P_{EXT} in rigid and flexible models, respectively. Hence, the relation between λ and $R_{MPFA,F+}$ (left) and the relation between λ and $R_{MPFA,F-}$ (right), are shown in Figure 7, accounting for all soil types. As a general trend the results show that, both for $R_{MPFA,F+}$ and $R_{MPFA,F-}$, at lower values of λ, the ratios approach to 1 for all soil types (despite that in some cases ratios in terms of PFAs between rigid and flexible models are higher than expected). This is a logical consequence of the proposed analysis, considering that for lower values of λ the flexibility should be negligible. Going to the higher values of λ, the ratios tend to decrease while the dispersion of the points tends to increases. Considering these observations, the best fitting option to correlate the two quantities resides in a power law with a negative exponent. In addition, by varying the soil categories the trends and the dispersions are comparable. Hence, the following empirical relationships can be estimated:

$$R_{MPFA,F+} = \lambda^{-0.75};\ for\ soils\ A, B, C \tag{4}$$

$$R_{MPFA,F-} = \lambda^{-0.8};\ for\ soils\ A, B, C \tag{5}$$

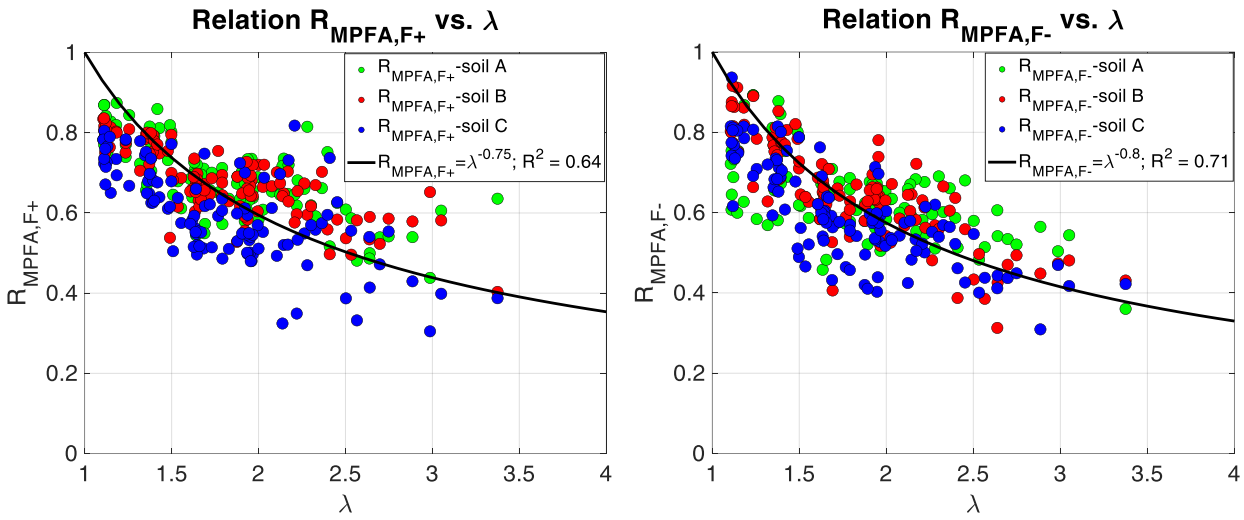

Figure 7 – The relation between λ and $R_{MPFA,F+}$ (left) and the relation between λ and $R_{MPFA,F-}$ (right), accounting for all soil types.

The close values of the exponents in Eqs. 4 and 5 suggest that, albeit there is a symmetry in the investigated structures, the increment of PFAs at P_{CEN} in flexible models is more consistent than the decrement of PFAs at P_{EXT}, as restated in some previous works, i.e., [15]. When it comes to the dispersion of the results, it is worth noting that there is a variation between the two cases (different coefficients of determination, R^2). On one hand, this is due to the consideration of the mean PFAs values and, on the other, due to the adopted modelling assumptions and the number of analyses.

3.2 Effects of nonlinearities on PFAs

The entire procedure described in the Section 3.1 was performed on the numerical models that account for nonlinearities, repeating the 7392 analyses on the flexible and rigid models. Obviously, in this Section the aim was not to describe the previously mentioned operations, but to perform the assessment of the proposed formulations empirically estimated on the linear elastic models, by highlighting the possible differences due to nonlinearities.

Firstly, a comparison between the time histories of the rigid and flexible diaphragm models could be of great interest, with and without nonlinearities. To address this issue, the results for the model previously

presented in Figure 5 are reported in Figure 8, showing the differences in terms of absolute accelerations for one of the considered records, for P_{CEN} of the rigid model and P_{CEN} and P_{EXT} of the flexible model. Considering the nature of the nonlinear numerical models, it can be seen that the recorded absolute accelerations are lower than the ones of the corresponding elastic models, due to the energy dissipation governed by the hysteretic behaviour.

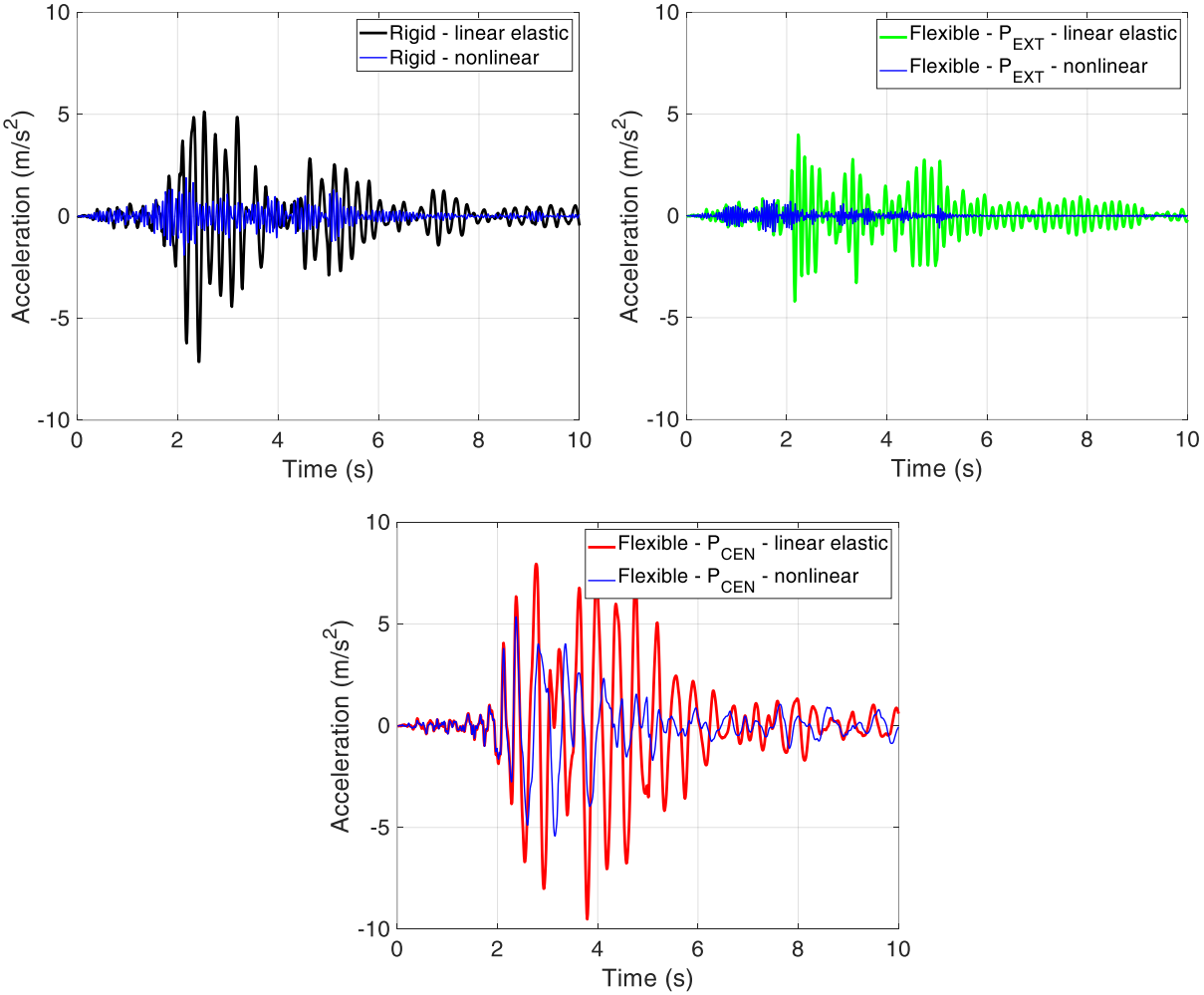

Figure 8 – Comparison of absolute acceleration time histories between the rigid and flexible models previously shown in Figure 5 for λ = 1.8 (only one ground motion record is shown herein). The value of the normalized yielding force (V/W) for the model amounts to 0.133.

Some observations can be highlighted. Namely, observing the differences at P_{CEN} of the flexible model, the response histories present some twists during the oscillation, given by the occurrence of yielding in members. Still, looking at the absolute values of the acceleration, larger values are always present at P_{CEN} of the flexible model, while at P_{EXT} of the flexible model lower values can be observed. Nevertheless, the differences between linear elastic and nonlinear models are more pronounced for P_{EXT} than for P_{CEN} of the flexible model. This effect is mainly due to a greater stiffness near P_{EXT}, which provokes a decrease in the displacement capacity. Exactly the opposite occurred for P_{CEN} of the flexible model, which had a higher flexibility with an increased displacement capacity. Finally, when it comes to the different swing phase between the linear elastic and nonlinear models, no conclusions can be provided, because it is strongly dependent from the applied hysteretic behaviour. On the other hand, some observations can be made by looking at the normalized yielding force (V/W), indicated in the caption of Figure 8, which applies to all models when nonlinearities are accounted for (V and W denote force and weight, respectively). Despite this value was not considered in the parametric analysis (and a specific trend cannot be traced), it could provide some insights into the transition from the elastic to nonlinear models. Looking at the models shown in Section 2.3, for $M_{\lambda MIN}$ the value of V/W equal to 0.16 was obtained (V = 86.5 kN; W = 540 kN), while for $M_{\lambda MAX}$ the value of V/W equal to 0.06 was observed (V = 335 kN; W = 5616 kN). Still, for $M_{\lambda LIM}$ the value of V/W equal to 0.08 was determined (V = 260 kN; W = 3240 kN) is observed. From the obtained values, it is possible to derive two main concepts: (a) by increasing the value of V/W, the differences between the elastic and nonlinear models decrease; (b) by increasing the flexibility, the V/W decreases and the differences between the elastic and nonlinear models increase.

Based on the obtained results, it is possible to replicate the proposed correlation shown in Figure 7, this time accounting for nonlinearities. The elaboration is shown in Figure 9, where the relations between λ and $R_{MPFA,F+}$ (left) and between λ and $R_{MPFA,F-}$ (right) are shown, accounting for all soil types.

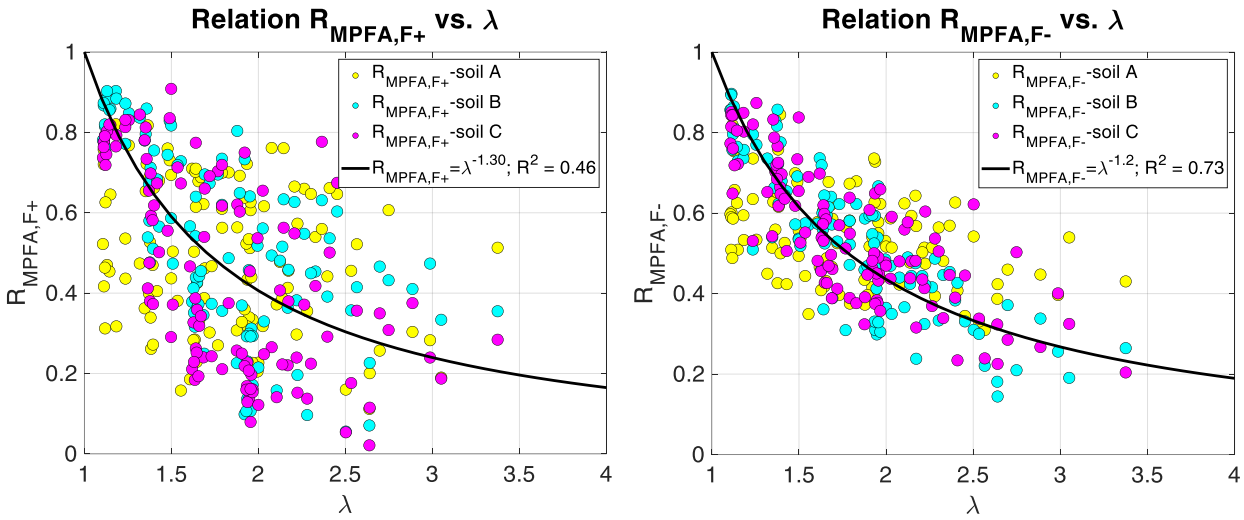

Figure 9 – The relation between λ and $R_{MPFA,F+}$ (left) and the relation between λ and $R_{MPFA,F-}$ (right), accounting for all soil types and nonlinearities in numerical models.

Observing the distribution for $R_{MPFA,F+}$, the dispersion is higher than the one previously obtained for the linear elastic cases, which suggests the strong influence of the nonlinearities on the PFAs at P_{CEN}. On the other hand, observing the distribution for $R_{MPFA,F-}$, the trend is enough clear and it follows the previously proposed power law with negative exponent (that is proposed also for $R_{MPFA,F+}$ with a low value of R^2). Regarding to the empirical correlations between the ratios and λ, the exponents of the power laws are different from the linear elastic cases, and Eqs. 4 and 5 can be re-edited as follows:

$$R_{MPFA,F+} = \lambda^{-1.30};\ for\ soils\ A, B, C \tag{6}$$

$$R_{MPFA,F-} = \lambda^{-1.20};\ for\ soils\ A, B, C \tag{7}$$

For both $R_{MPFA,F+}$ and $R_{MPFA,F-}$, the value of the exponent decreases, showing that for higher values of λ the variation in terms of PFAs between flexible and rigid models increases, mainly due to a different behaviour of the two modelling assumptions under horizontal actions, especially when nonlinearities are accounted for.

4. FLOOR RESPONSE SPECTRA

4.1 Estimation of FRS ratios between rigid and flexible diaphragm buildings

To estimate FRS differences at floors of the models having rigid and flexible diaphragms, a linear elastic single-degree-of-freedom (SDOF) oscillator was considered for a NSC model, assuming mass and stiffness according to periods of vibration ranging from 0 to 4.0 s. A fixed value of 5% damping was assumed for NSCs. Nonlinearity of the NSCs was not considered since the focus of the paper is the diaphragm flexibility. Thus, FRS were computed for all linear elastic models and for all applied ground motions, accounting for the three scenarios investigated for PFAs: (1) at P_{CEN} of models with rigid diaphragms, indicated as FRS_R; (2) at P_{CEN} of models with flexible diaphragms, indicated as FRS_{F+}; (3) and at P_{EXT} of models with flexible diaphragms, indicated as FRS_{F-}.

The mean of FRS for each model and each scenario was evaluated and the results are shown in Figure 10. Four graphs are reported showing 112 FRS for each soil type and for each floor modelling assumption, reporting accelerations in unit of *g* and scaling *Y* axis to improve visibility (all next figures reporting FRS adopt these plotting criteria). Also, a zoom on the peaks for the FRS of soil B is presented, where two main effects can be seen. In fact, comparing FRS_R and FRS_{F-}, higher peaks for models with rigid diaphragms occurred, as well as a shift of the resonance zone to the left. In opposite, comparing FRS_R and FRS_{F+}, lower peaks for models with rigid diaphragms can be seen, along with a shift to the right of the resonance zone. These effects were investigated and discussed below (Sections 4.1.1 and 4.1.2), by quantifying variations with regard to the flexibility, while a focus on the physics under the obtained results is reported in Section 4.2, where also nonlinearities are accounted for.

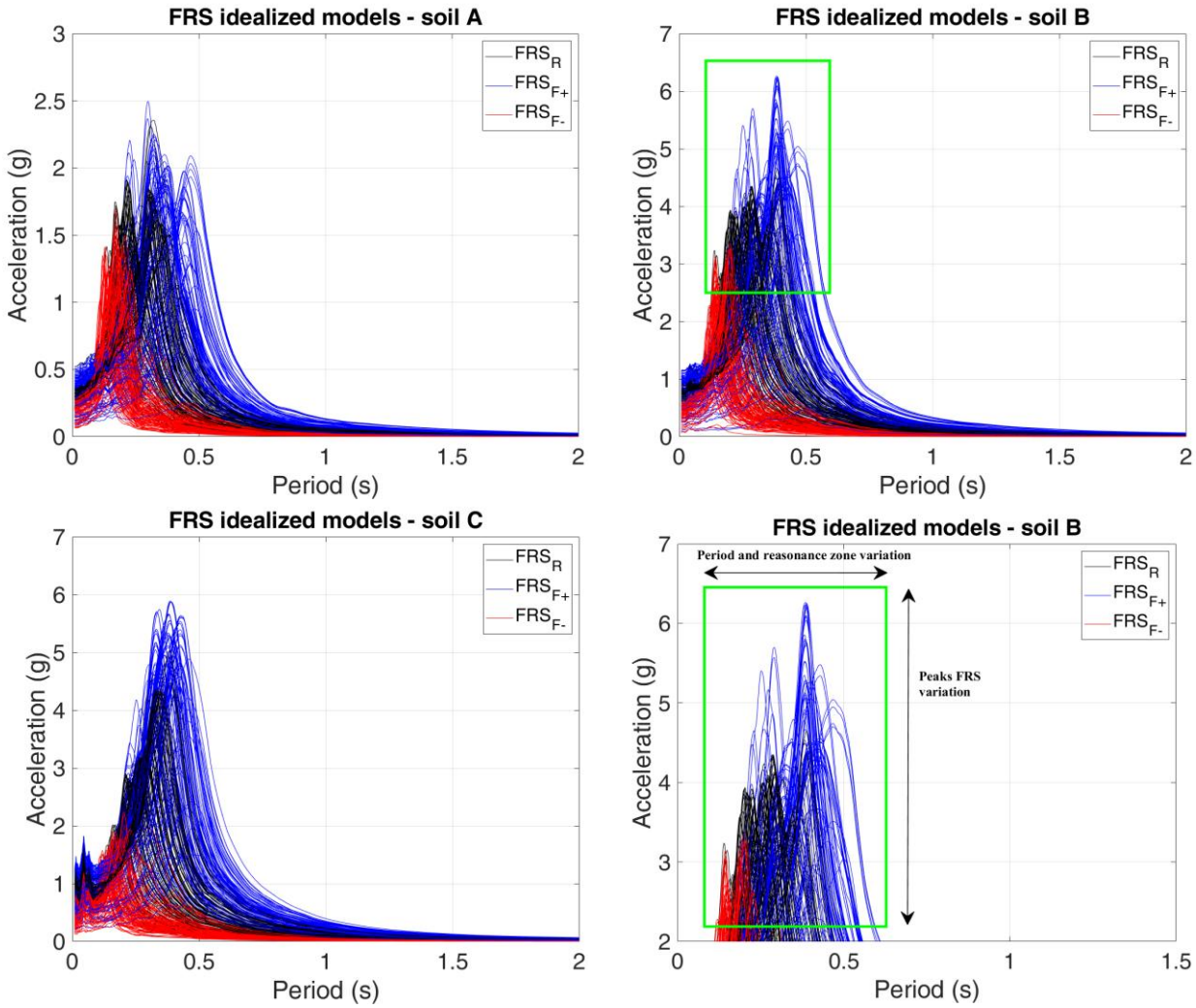

Figure 10 – FRS for P_{CEN} of models with rigid diaphragms, FRS_R; P_{CEN} of models with flexible diaphragms, FRS_{F+}; P_{EXT} of models with flexible diaphragms, FRS_{F-}, for soils A, B and C; Zoom on FRS graph of soil B (green box), indicating the variation of peaks in the resonance zone.

4.1.1 Period and resonance zone variation

In order to investigate the resonance zone shifting, some preliminary considerations must be outlined. Firstly, as shown in several studies, the diaphragm flexibility indicates the well-known effect of the period lengthening, which is the main cause of the FRS resonance zone position variation. In this case, it is clear that the increase in acceleration at P_{CEN} (as observed for PFAs) is due to a greater flexibility than in the

corresponding rigid diaphragm model, which leads to the period increase. Likewise, the decrease in acceleration at P_{EXT} is due to a lower flexibility than in the corresponding rigid diaphragm model, which leads to the period decrease. Hence, the parametrization of this effect must be sought in the period variation among rigid and flexible diaphragm models and, to be in accordance with a practical approach, it needs to be related to λ.

To this scope, another parameter can be identified for each model, which is the effective FRS resonance zone variation, evaluated by observing the peak shifting, indicated as $R_{T,RZ+}$ and $R_{T,RZ-}$ and defined as the ratios between the periods of the peaks of FRS_R ($T_{P,R}$) and FRS_{F+} ($T_{P,F+}$), and between the periods of the peaks of FRS_{F-} ($T_{P,F-}$) and FRS_R ($T_{P,R}$), respectively:

$$R_{T,RZ+} = \frac{T_{P,R}}{T_{P,F+}}; R_{T,RZ-} = \frac{T_{P,F-}}{T_{P,R}} \tag{8}$$

Furthermore, a relation can be established among the values of $R_{T,RZ+}$ and $R_{T,RZ-}$ and λ. The trend is shown in Figure 11, where for lower values of λ, $R_{T,RZ+}$ and $R_{T,RZ-}$ approach to 1, while for higher values of λ, they increase with a slower and slower speed, for each soil type.

Hence, the best shape of the correlation among the observed parameters is again a power law with a negative exponent, as following:

$$R_{T,RZ+} = \lambda^{-0.6};\ for\ soils\ A, B, C \tag{9}$$

$$R_{T,RZ-} = \lambda^{-0.8};\ for\ soils\ A, B, C \tag{10}$$

As in the previous empirical relationships, the exponents have different values, which is an occurrence that once again suggests that the symmetry of the investigated flexible models does not provide similar behaviour between floor demands at P_{EXT} and P_{CEN}. It should be noted though the shifting of the resonance zone does not seem to be affected by the applied set of input accelerograms (e.g., soil type). It is influenced by the dynamic properties of the investigated buildings, by considering the strong dependence of the T variation in the considered direction (Y).

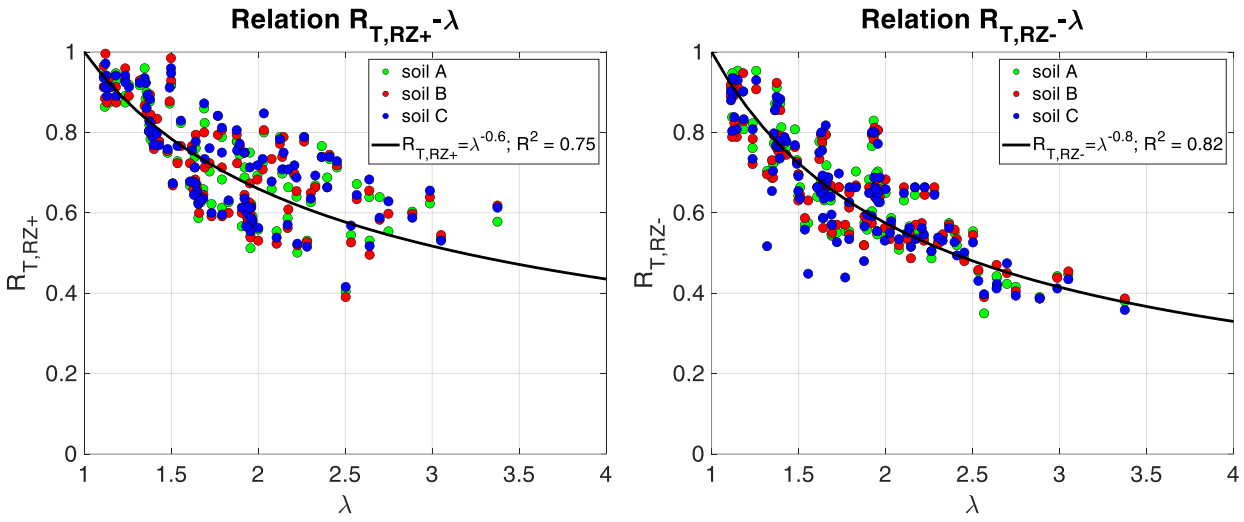

Figure 11 – Relations between λ and $R_{T,RZ+}$ (left) and λ and $R_{T,RZ-}$ (right), accounting for all soil types.

4.1.2 Variation of FRS peaks

Regarding the observed variation of FRS peaks in Figure 10, some differences can be distinguished from the discussion on the resonance zone shifting. In this case, it was observed that the seismic input plays a key role considering that the amplifications of the peaks in the resonance zone are strongly related to the applied ground motions. Also, the soil category is a paramount factor, considering that the absolute accelerations can decrease or increase according to the input properties (e.g., frequency content, peak ground acceleration). In fact, FRS peaks of soil A are lower than the ones for soils B and C. In addition, some peaks for soil B exceed the maximum values given by the ones for soil C, even if this occurs for sporadic cases. Nevertheless, the ratio approach adopted in this paper could overcome the differences in terms of peaks, providing also a unique relationship with the flexibility parameter for different soil types. Thus, in order to estimate the FRS peak variation between rigid and flexible diaphragms, the terms R_{PF+} and R_{PF-} are defined, and they indicate the ratio between acceleration peaks of FRS_R ($S_{e,PR}$) and FRS_{F+} ($S_{e,PF+}$) and the ratio between acceleration peaks of FRS_{F-} ($S_{e,PF-}$) and FRS_R ($S_{e,PR}$), respectively:

$$R_{PF+} = \frac{S_{e,PR}}{S_{e,PF+}}; R_{PF-} = \frac{S_{e,PF-}}{S_{e,PR}} \quad (11)$$

The values of R_{PF+} and R_{PF-} were correlated to λ values and the results can be observed in Figure 12 where, as expected, for the values of λ close to 1, the peaks of FRS in the two modelling assumptions present the same values (R_{PF+} and R_{PF-} close to 1). Increasing the value of λ, R_{PF+} and R_{PF-} decrease at a constant rate, which suggests a linear trend of the ratios. Even in this case, the soil category does not influence the trend and the scattered points present a distributed amplitude between 0 and 1.

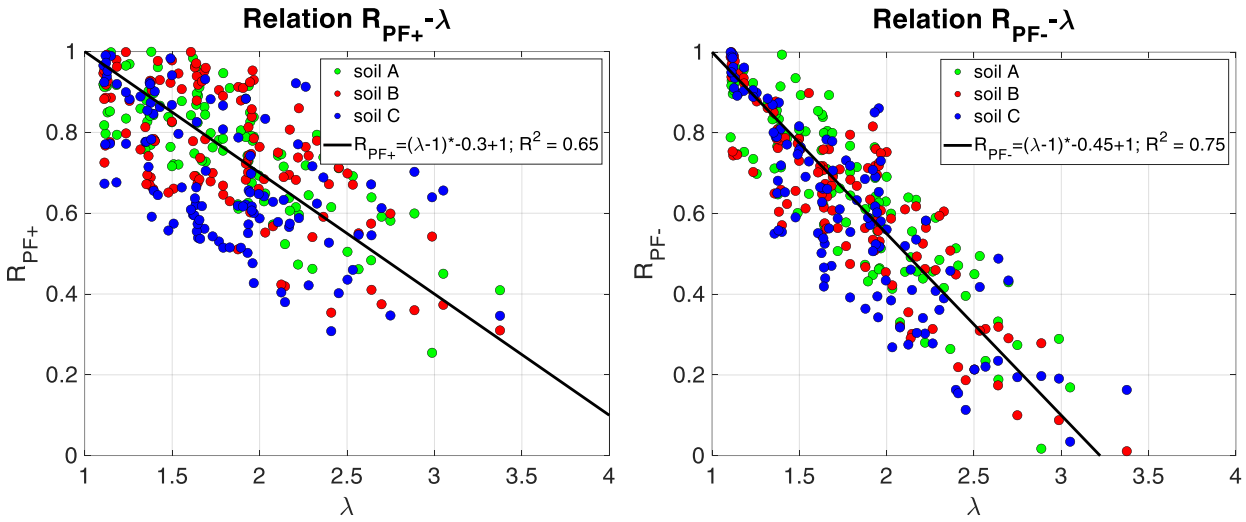

Figure 12 – Relations between λ and R_{PF+} (left) and λ and R_{PF-} (right), accounting for all soil types.

Considering that the linear trend must go through 1 for both quantities in the graphs, the following fittings are defined:

$$R_{PF+} = -0.30 \cdot (\lambda - 1) + 1;\ for\ soils\ A, B, C \tag{12}$$

$$R_{PF-} = -0.45 \cdot (\lambda - 1) + 1;\ for\ soils\ A, B, C \tag{13}$$

It is worth noting that, for the expression of R_{PF-}, very few results are out of the expression in Eq. 13 (see Figure 12, right), which provide a limitation in the use of the relationship. On the other hand, as practical suggestion, for higher values of λ, a low value of R_{PF-} can be assumed (e.g., the result obtained from a λ=3.2, which return R_{PF-} equal to 0.01). In the end, it is worth remembering that the proposed formulations are valid for single-storey buildings having period of vibrations ranging from 0.05 to 0.45 s, as typical of RC buildings, and that they will be validated with the case study example reported in Section 5.

4.2 Effects of nonlinearities on FRS

As was done for PFAs, FRS were evaluated on single-storey models accounting for structural nonlinearities. In Figure 13 are shown FRS at P_{CEN} of models with rigid diaphragms, FRS_R; at P_{CEN} of models with flexible diaphragms, FRS_{F+}; and at P_{EXT} of models with flexible diaphragms, FRS_{F-}. It can be seen how the situation substantially changes compared to the linear elastic cases, also accounting for each soil category.

For example, looking at the acceleration peaks, this time higher values can be observed for soil C. In order to assess the formulations proposed for the linear elastic case in a view of the resonance zone and FRS peak variation, in Figure 14 is shown the vis-à-vis comparison among FRS for linear elastic and nonlinear structures, separately for FRS_R, FRS_{F+} and FRS_{F-} (where the nonlinear cases are represented in green and the period range is limited to 1.5 s), for soil B (similar was observed for other soil categories). The results show that the FRS shapes are not similar in the linear elastic and nonlinear cases, which suggests the impossibility to adopt the formulations proposed in Sections 4.1.1 and 4.1.2 for the resonance zone shifting and the FRS peak variation.

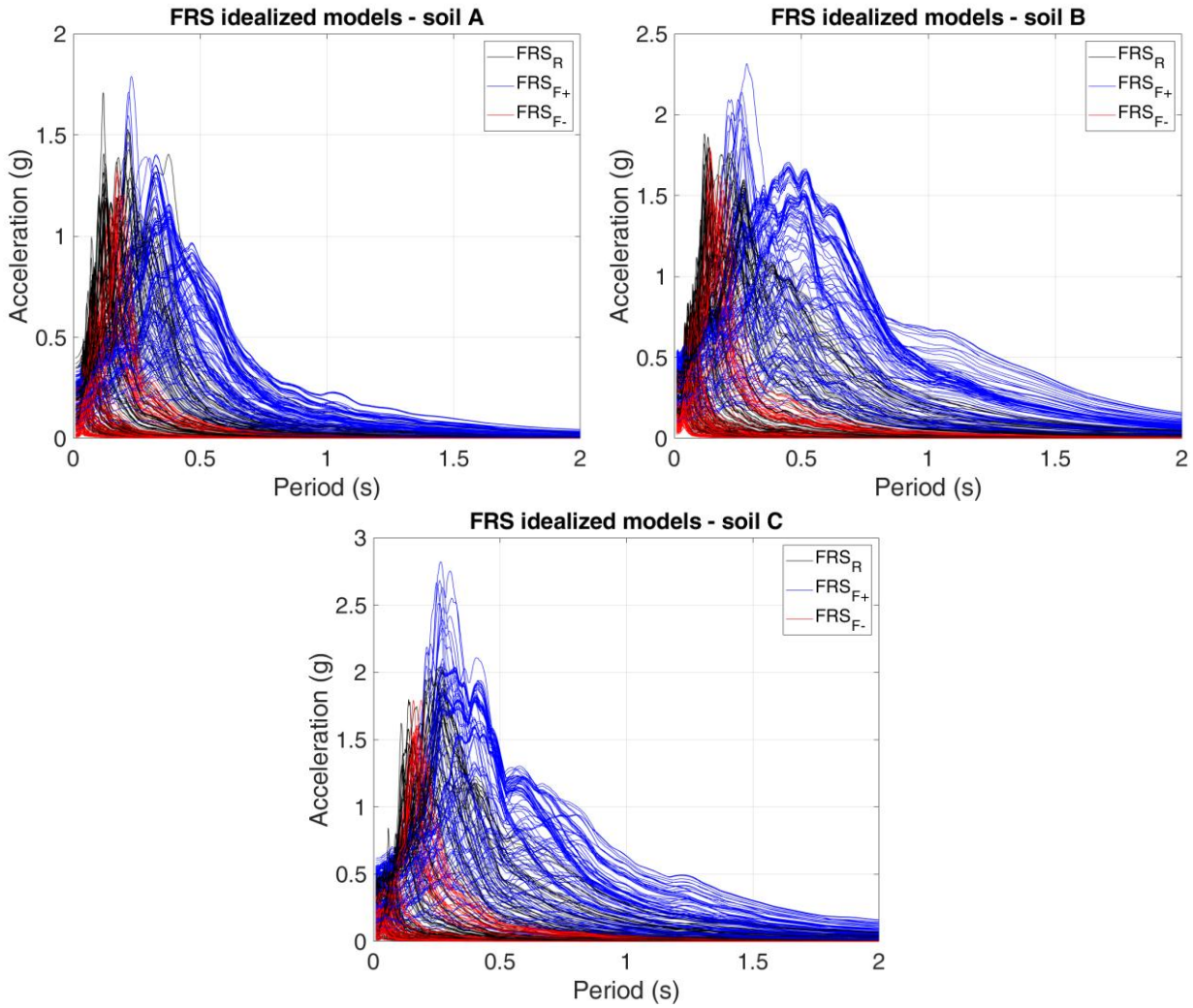

Figure 13 – FRS for P_{CEN} of models with rigid diaphragms, FRS_R; P_{CEN} of models with flexible diaphragms, FRS_{F+}; P_{EXT} of models with flexible diaphragms, FRS_{F-}, for all soil types and accounting for nonlinearities.

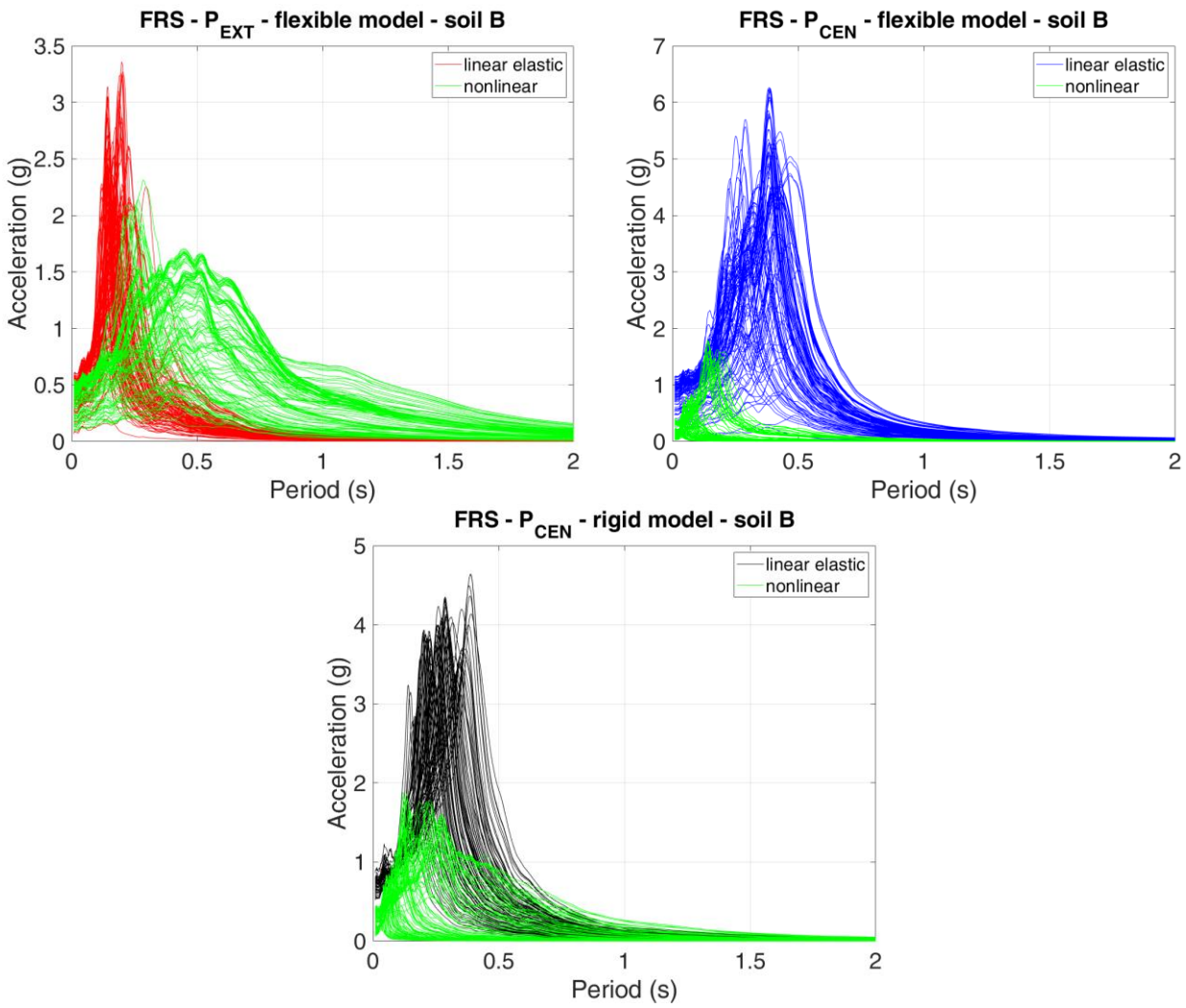

Figure 14 – Comparison of FRS in structures with and without nonlinearities at P_{CEN} of models with rigid diaphragms, FRS_R; at P_{CEN} of models with flexible diaphragms, FRS_{F+}; at P_{EXT} of models with flexible diaphragms, FRS_{F-}, for soil type B.

By looking at the graphs in Figures 13 and 14, some aspects can be distinguished, in order to define the physics and to provide some practical insights. In general, as observed for PFAs, the values of FRS peaks in nonlinear models are lower than the ones obtained for the linear elastic models, despite this difference is less pronounced for FRS_R and FRS_{F-} and more pronounced for FRS_{F+}. In general, in FRS graphs for linear elastic and nonlinear models two peaks for flexible structures are present instead of one, i.e., FRS at P_{EXT}

and P_{CEN}, given by a different behaviour of the two structural parts (higher flexibility induces lower frequency).

In some cases, FRS_{F+} have two peaks instead of one (more or less visible in Figure 14), which implies the occurrence of an additional degree-of-freedom (DOF). In other cases, the peak values of FRS_{F-} seem to be similar in terms of amplitude than the ones from FRS_R. Regarding the resonance zone shifting, it can be seen that higher peaks for FRS_R and FRS_{F-} occur in the same period range, while the ones for FRS_{F+} are in a similar position as in the linear elastic case. All these aspects can be summarized by considering what happens in the case of yielding of structural elements. For the flexible models, the seismic action likely leads to the first yielding in central columns (as shown in [27,28,37]), which evolves in a stiffness redistribution within the system that in turn provides a different distribution of the input acceleration on structural elements. The latter can provide an increase in acceleration of external elements (higher FRS peaks at P_{EXT}), and an additional DOF with higher frequency. At the same time, the occurrence of yielding in central elements does not influence the resonance zone of FRS_{F+}, but only affects FRS peak values. Regarding to the rigid models, the occurrence of yielding (likely in the central part, as for the flexible diaphragm cases) again leads to a higher frequency of the additional DOF, which is related to higher FRS peaks but, at the same time, the initial FRS peaks still remain close to the period observed in the linear elastic cases. The extreme proximity of the peaks for FRS_R and FRS_{F-} reveals that after the linear elastic response, the models with rigid and flexible diaphragms tend to have similar periods and behaviour under seismic excitation (as occurs for torsion). Hence, the results imply that what actually happened is that the nonlinear SDOF structures can vibrate in two modes and, by judging the reduction of FRS values, especially in the resonance zone, the well-known fact that nonlinear structural behaviour decreases the FRS. Additionally, the occurrence of the second-mode FRS peaks (as in some FRS_{F+} cases) imply that (1) structural response in the second mode was elastic, which is a common assumption in seismic analysis and design, and (2) there was a possible transfer of energy from the first to the second mode as, for example, observed in [49].

After the above observations, the steps performed on the peaks FRS of linear elastic models were repeated for nonlinear models. Thus, the relations among the values of $R_{T,RZ+}$ and $R_{T,RZ-}$ and λ were again estimated, according to the distribution of the values reported in Figure 15. In this case, it can be seen that despite the lower values, the differences between rigid and flexible models tend to increase, following a well-defined trend. In fact, in both cases in Figure 15, a power law rules the variation of $R_{T,RZ+}$ and $R_{T,RZ-}$ in the function of λ. Hence, the exponents of both relations were recomputed and Eqs. 9 and 10 were re-edited as follows:

$$R_{T,RZ+} = \lambda^{-2.5};\ for\ soils\ A,B,C \tag{14}$$

$$R_{T,RZ-} = \lambda^{-1.2};\ for\ soils\ A,B,C \tag{15}$$

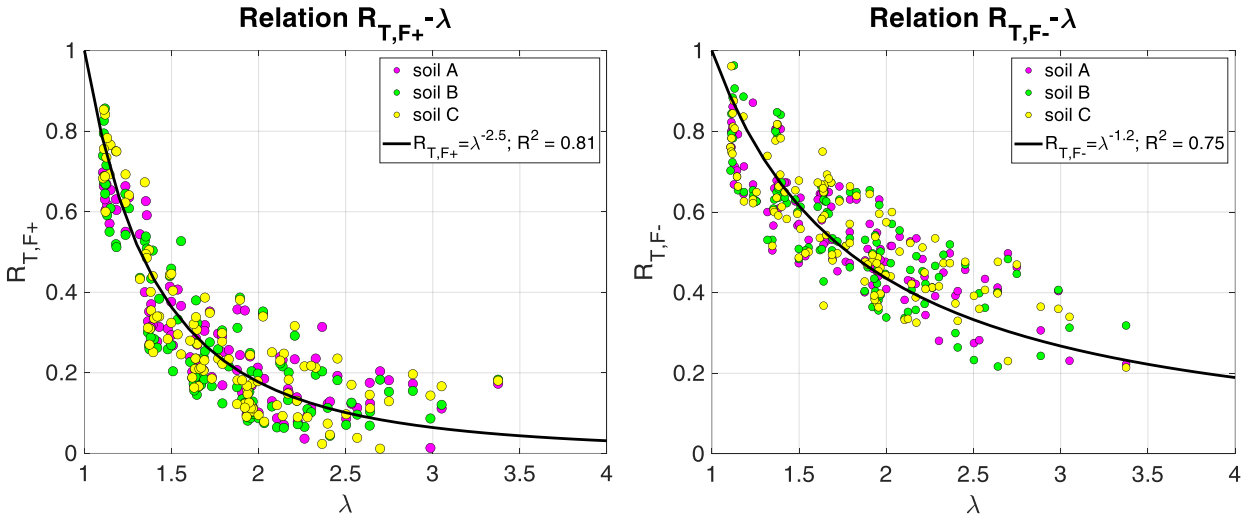

Figure 15 – Relations between λ and $R_{T,RZ+}$ (left) and λ and $R_{T,RZ-}$ (right), accounting for all soil types and structural nonlinearities.

The exponent of the Eq. 14 is significantly changed respect to the value in the linear elastic case, while the change of the same term in Eq. 15 is smaller. In general, the dispersion is not high for the peaks' shifting, which is confirmed by the high values of R^2 for both cases. Similar was performed for FRS peaks, where the nonlinear results are reported in Figure 16, showing the relations between R_{PF+} and R_{PF-} and λ. The fittings of the two sets of points, accounting for all soil types, are expressed as follows:

$$R_{PF+} = -0.45 \cdot (\lambda - 1) + 1;\ for\ soils\ A, B, C \tag{16}$$

$$R_{PF-} = -0.40 \cdot (\lambda - 1) + 1;\ for\ soils\ A, B, C \tag{17}$$

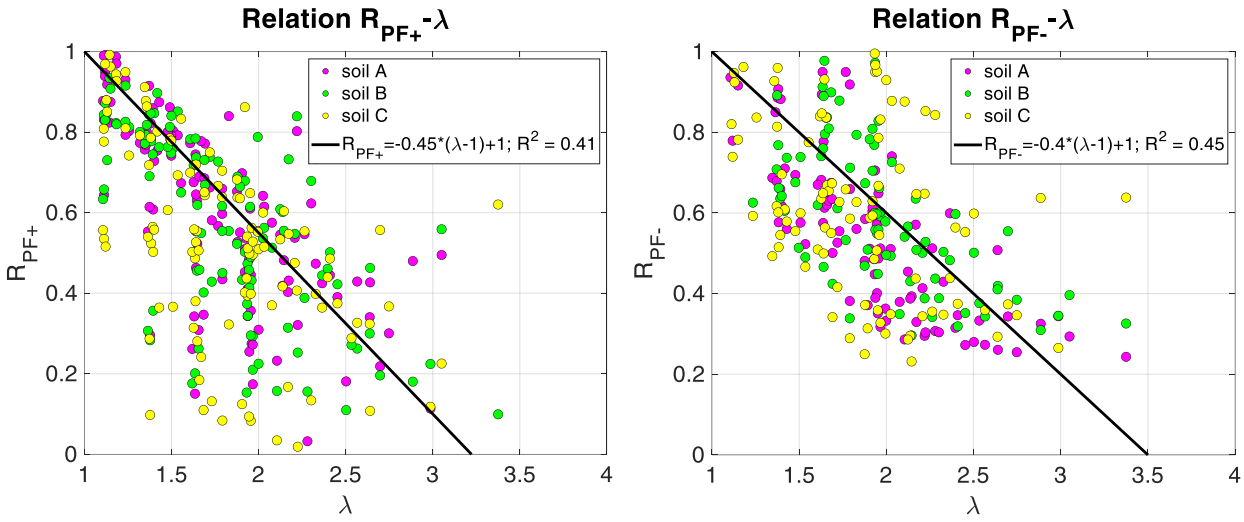

Figure 16 – Relations between λ and R_{PF+} (left) and λ and R_{PF-} (right), accounting for all soil types and structural nonlinearities.

By looking at the results in Figure 16, the obtained dispersion is high in both cases (values of R^2 lower than 0.5), but in the authors' opinion this depends on the strong influence of nonlinearities and the properties of the applied ground motion records. Nevertheless, the best fitting option is the linear one, because it works for the linear elastic case and provides a good relation from the practical point of view. In addition, the obtained exponents are similar, which is in line with the outcomes observed from Figure 12.

In the following text the defined rules were tested and applied *as is* on a case study example, but additional further analyses could change the values of the exponents. Finally, in an overarching vision of the focused problem, the adopted methodology that quantify ratios of PFAs and FRS between rigid and flexible models can provide the basis for modifying code formulas and practice-oriented approaches for the PFA and FRS estimation.

5. CASE STUDY EXAMPLE

The case study example is an existing RC school building located in Southern Italy, Puglia region. The building is a part of a scholastic complex made in the early 80's, and it was designed only for gravity loads. It has a rectangular in-plane shape, having dimensions of 10 m in *Y* direction and 45 m in *X* direction. The building is a single-storey moment-frame structure, 3.80 m high, and with masonry infills along the external sides. The moment-frames in *X* direction are spaced at 5 m (10 columns), while only two external moment-frames are present in *Y* direction, having a smaller bay of 3 m and a larger one of 7 m. The orientation of the slab is in *Y* direction, and it is of the same typology of the idealized buildings described in Section 2.1. The summary of geometrical and mechanical parameters of the case study example, with regard to structural and non-structural elements, are indicated in Table 3, where it is worth nothing that the reported values are the output of accurate in-situ investigations, which allowed an achievement of a comprehensive knowledge level (according to [50]). Dead and live loads were assumed to be equal to 6 and 3 kN/m^2, respectively.

When it comes to modelling of the case study building, two nonlinear numerical models were established, with and without diaphragm flexibility. The modelling approach was completely the same as the one described in Section 2.1, considering a lumped plasticity for structural elements and two elastic cross braces for the simulation of the diaphragm flexibility. The only addition was the masonry infill modelling, for which two cross braces were used, modelled with *corotationalTruss* elements, and their slenderness and nonlinear constitute laws were computed according to [51] and [52], respectively, simulating only their in-plane behaviour. In the end, no brittle mechanisms were considered, such as shear and joint failures, in order to avoid the addition of other variables in the problem under investigation.

Firstly, eigenvalue analyses were performed on numerical models, showing that the main three periods of vibration for the models with and without flexible diaphragm were slightly different. As expected, the main difference was obtained for the fundamental periods of vibration, which is in *Y* direction, and which amounted to 0.128 s for the model with the flexible diaphragm and to 0.091 s for the model with the rigid diaphragm. In Figure 17 the meshes of the two numerical models are shown (with the indication of reference axes), and the deformed shapes related to the fundamental periods of vibrations, which demonstrate how

the in-plane deformed shapes change and, above all, how the deformed shape of model with flexible diaphragm looks like an in-plane parabola (or an arch).

Table 3 – Geometrical and mechanical parameters of the case study building example

Geometrical parameters	Mechanical parameters of structural elements	Mechanical parameters of masonry infill panels
Internal columns: 40 cm x 40 cm - 4Φ18, Φ6/20 cm External columns: 60 cm x 40 cm - 6Φ18, Φ6/20 cm Internal beams: 30 cm x 40 cm - 4Φ16, Φ6/18 cm External beams: 30 cm x 40 cm - 4Φ16, Φ6/18 cm	Compressive strength of concrete: 18 MPa Tensile strength of steel reinforcement: 422 MPa Elastic modulus of concrete: 26.9 GPa Elastic modulus of reinforcing steel: 210 GPa	Vertical elastic modulus of masonry: 3080 MPa Diagonal elastic modulus of masonry: 1495 MPa Shear modulus of masonry: 1233 MPa Tensile strength of masonry: 0.36 MPa Compression strength of masonry: 2.5 MPa

For the model with the flexible diaphragm, the value of λ was evaluated by applying a horizontal static load case by means of a system of forces with unitary resultants acting at each node, and its value amounted to 2.25. This implies that, according to [26], the floor can be classified as flexible, and the empirical formulations proposed in this paper can be tested on this realistic case study example. To this aim, the set of records employed for soil type A was used to run nonlinear dynamic analyses. The selected records were applied one at a time in Y direction, in order to estimate PFAs and FRS on rigid and flexible diaphragm models (observed values), and to assess the accuracy of the analogous quantities (estimated values) from the proposed formulations. Histograms reporting the observed values are reported in Figure 18, for each record, of $R_{MPFA,F+}$ (left), and $R_{MPFA,F-}$ (right), at P_{CEN} of the rigid model and at P_{CEN} and P_{EXT} of the flexible

model. Black horizontal line shows the estimated values obtained by applying Eqs. 6 and 7 for $\lambda = 2.25$, and they are equal to 0.35 ($R_{MPFA,F+}$) and 0.38 ($R_{MPFA,F-}$).

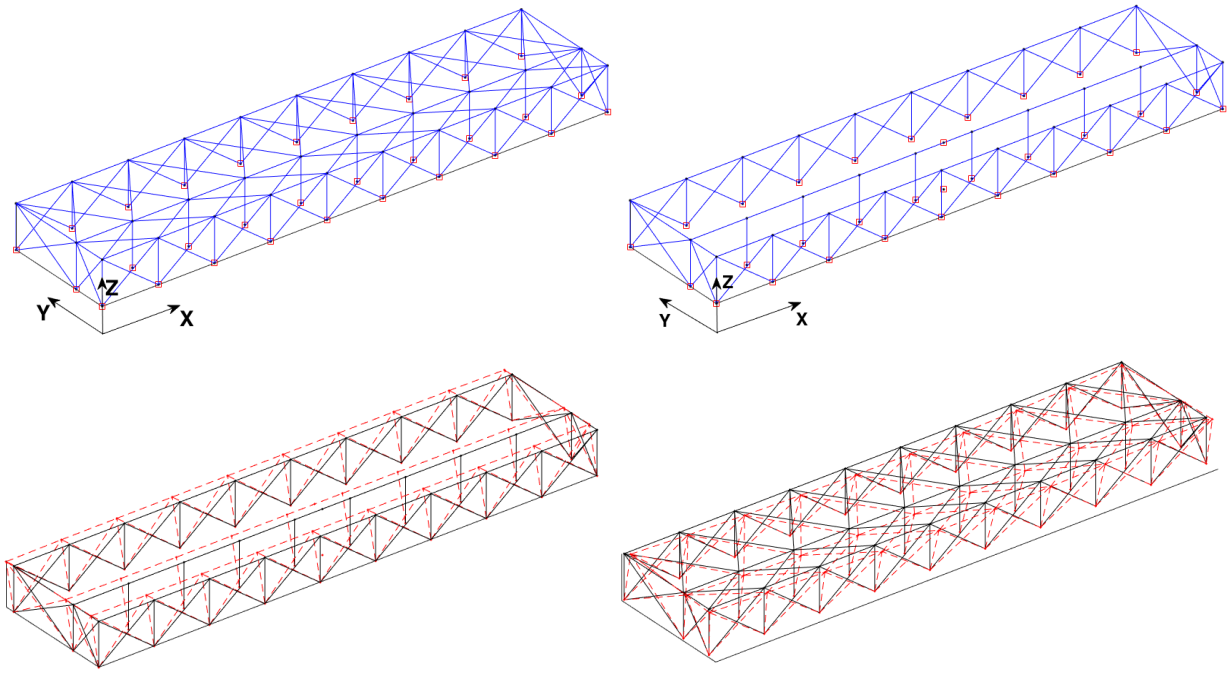

Figure 17 – 3D view of the numerical models for the case study building example, with and without diaphragm flexibility and the indication of the main reference axes. The eigenvectors related to the first period of vibration for both models are shown below (in both cases, in *Y* direction).

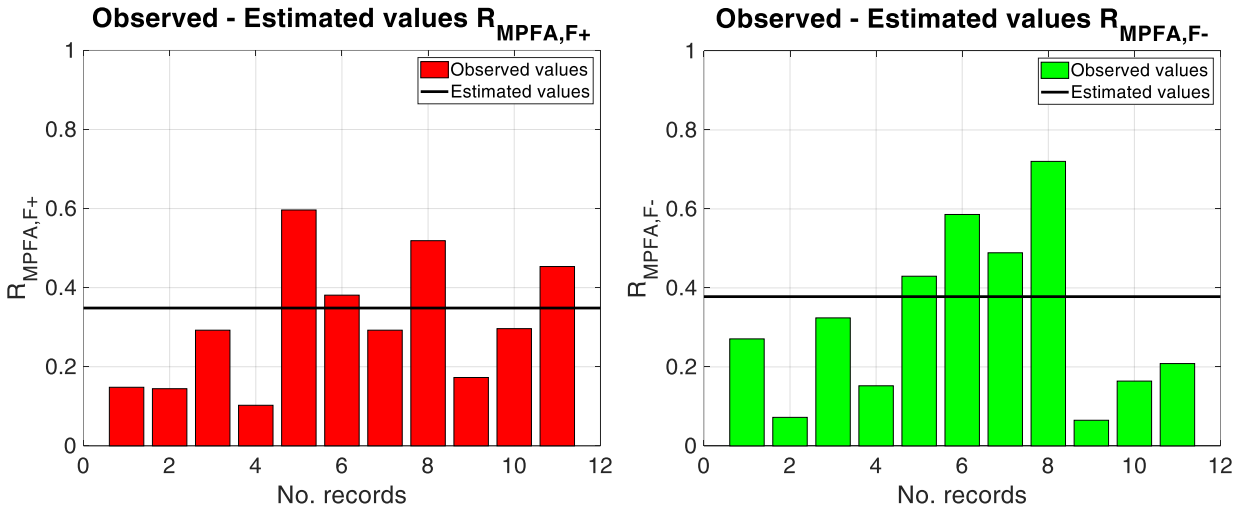

Figure 18 – Histograms reporting the observed $R_{MPFA,F+}$ (left) and $R_{MPFA,F-}$ (right), and black lines indicate the estimated values.

As observed, the black lines provide medium estimates of the PFAs results, revealing that the proposed approach is appropriate in most cases. In addition, to evaluate the accuracy of the estimated values, it is possible to compare them with the observed means of $R_{MPFA,F+}$ and $R_{MPFA,F-}$, as obtained by the applied records. In particular, the observed mean value of $R_{MPFA,F+}$ amounted to 0.31, while the mean value of $R_{MPFA,F-}$ amounted to 0.32. Thus, the accuracy of the proposed formulation, for this case, is equal to about 11% and 16% for $R_{MPFA,F+}$ and $R_{MPFA,F-}$, respectively, with the estimated values being larger than the observed ones.

Furthermore, FRS were evaluated for both rigid and flexible diaphragm models. The obtained results are shown in Figure 19, accounting for each record (left) and for the mean FRS (right), evaluated at P_{CEN} of the rigid model and at P_{CEN} and P_{EXT} of the flexible model. It can be seen in Figure 19, left, that the trend is similar to the one from Figure 13, with a similar position of the resonance zone for FRS_R and FRS_F, and higher peak values of FRS_{F+} than FRS_R and FRS_{F-}. Also, by looking at the mean FRS, the above observations regarding two peaks are confirmed, and the proposed formulations (accounting for nonlinearities) can be tested, in order to evaluate their accuracy.

Regarding the comparisons, the evaluations between the observed and estimated values was performed by considering FRS peaks for FRS_R, FRS_{F+} and FRS_{F-}. As for the resonance zone variation, the observed values of periods in the peaks of FRS_R, FRS_{F+} and FRS_{F-} were equal to 0.10, 0.48 and 0.04 s, respectively. Hence, using the observed values, $R_{T,RZ+}$ and $R_{T,RZ-}$ amounted to 0.20 and 0.44. By using $\lambda = 2.25$ in Eqs 14 and 15, the estimated values of $R_{T,RZ+}$ and $R_{T,RZ-}$ were obtained and they amounted to 0.13 and 0.38, respectively. Comparing the observed and estimated values, the obtained accuracy is of 35.29% and 14.85% for the resonance zone period of FRS_{F+} and FRS_{F-}, respectively. The results show an acceptable inaccuracy of the proposed approximate empirical formulation.

As for the FRS peak variation, the observed values FRS_R, FRS_{F+} and FRS_{F-} peaks were equal to 0.42 g, 0.81 g and 0.16 g, respectively. Hence, using the observed values, R_{PF+} and R_{PF-} amounted to 0.39 and 0.52. By using $\lambda = 2.25$ in Eqs. 16 and 17, R_{PF+} and R_{PF-} were obtained and they amounted to 0.44 and 0.50, respectively. Comparing observed and estimated values, the obtained accuracy is 11.8% and 3.1%.

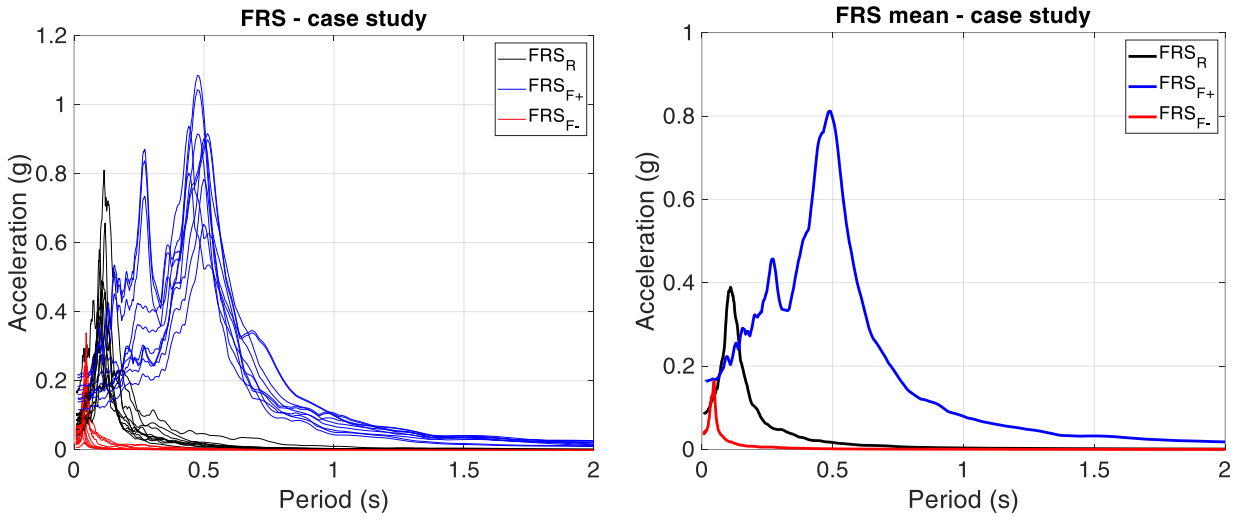

Figure 19 – FRS at P_{CEN} of the model with rigid diaphragm, FRS_R; P_{CEN} of model with flexible diaphragm, FRS_{F+}; P_{EXT} of the model with flexible diaphragm, FRS_{F-} (left); mean of all FRS (right)

In the end, despite the obtained differences, the above proposed formulations could open new scenarios in this field, in order to provide an overall estimate of FRS variations when a diaphragm flexibility occurs. Still, the proposed formulations are calibrated with a limited number of records, which governs the obtained results. Further developments consist in the assessments of the proposed empirical results with more sets of ground motion records and different building configurations.

6. CONCLUSIONS

This paper presents a study about the influence of diaphragm flexibility on peak floor accelerations (PFAs) and floor response spectra (FRS) for investigating the behaviour of acceleration sensitive non-structural components. The study was performed on a large sample of idealized single-storey RC regular buildings, in which some geometrical parameters were changed for the purpose of a parametric analysis on a large number of simulated buildings. Three sets consisting of 11 ground motion records each were employed as the seismic input, in order to assess the influence of different seismicity levels on the focused topic. Different numerical models were established, in order to simulate the diaphragm flexibility and to check

the influence of nonlinearities. The results of the study provided empirical formulations for the estimation of the ratios between PFAs and FRS in single-storey RC buildings with rigid and flexible diaphragms, and they were tested on an existing case study building. All proposed formulations correlate the variations of PFAs and FRS with the diaphragm flexibility, through the use of the in-plane displacement ratio, λ. The detailed outcomes of the study can be summarized as follows:

1. The PFA values obtained for models with flexible diaphragms increased and decreased with respect to their theoretical counterparts with rigid diaphragms. In detail, the more flexible parts of buildings, identified at P_{CEN}, exhibited higher PFAs, while the more rigid parts of buildings, identified at P_{EXT}, had lower PFAs. Opting for a ratio approach to quantify the variation in terms of PFA values obtained from the rigid and flexible diaphragm models, it was observed that the PFA variation increased for higher values of λ with a power law. This was observed for all (different) seismic input levels since a ratio approach is not influenced by the seismic intensity. Overall, nonlinearities of numerical models produced lower PFA values but, at the same time, no substantial differences in trend could be observed.
2. Diaphragm flexibility produced two main effects on FRS: (1) a shift of the FRS resonance zone; (2) a variation of the FRS peak values. As for the first effect and with regard to the results obtained for the rigid diaphragm models, FRS evaluated at P_{CEN} in the linear elastic models exhibited shifting of the resonance zone to the left (shorter periods), while FRS evaluated at P_{EXT} exhibited shifting of the resonance zone to the right (longer periods). Similar outcomes were obtained for nonlinear models, where the resonance zones of the rigid diaphragm models and at P_{EXT} of the flexible diaphragm models were in a similar position, while the resonance zone at P_{CEN} of the flexible diaphragm models shifted to the right. Still, the different input for different soil types did not influence the shifting of the resonance zone in any case. When it comes to the second effect and considering the results obtained for the rigid diaphragm models, for the linear elastic models FRS peaks had higher values at P_{CEN} in the flexible diaphragm models and lower values at P_{EXT} in the flexible diaphragm models. Also, by looking at different ground motion record sets, similar trend

was observed. Similar outcomes were obtained for the nonlinear models. In addition, the diaphragm flexibility produced an important effect on the FRS peaks, which was reflected through an additional peak related to an additional DOF with the respect to the linear elastic case: an effect that is anyway related to different FRS by monitoring P_{EXT} and P_{CEN} in the flexible models. In both linear elastic and nonlinear cases, the adopted ratio approach provided different trends for the resonance zone shifting (power law) and for the position of the FRS peaks (linear law), for which empirical formulas are proposed.

This study provides some practical insights to account for the diaphragm flexibility in single-storey RC buildings where this effect is most significant. Nevertheless, some additional steps are necessary to provide a full definition of the problem. Firstly, as many times repeated throughout the manuscript, analyses should be carried out by using other sets of ground motion records, in order to identify the effect of different seismicity levels and to calibrate different values of variables in the proposed empirical equations. Afterwards, the proposed formulations should be employed in a code-oriented approaches, in order to estimate the PFA and FRS variation by knowing λ, and by referring to more structural configurations. To this scope, it is necessary to enlarge the set of buildings, by assessing the proposed formulations on multi-storey buildings, where it is expected that the diaphragm flexibility effect decreases. Still, the influence of the yielding force on PFAs and FRS should be investigated further, including different levels of the V/W values, especially when nonlinear models are analysed. In the end, further studies are required for accounting the conjunct effects of diaphragm flexibility with other irregularity sources, such as torsion.

Declaration of competing interest

The authors declare that they have no known competing financial interests or personal relationships that could have appeared to influence the work reported in this paper.

Acknowledgements

The first author acknowledges funding by Italian Ministry of University and Research, within the project 'PON-Ricerca e Innovazione-2014–2020, CODICE CUP (D.M. 10/08/2021, n. 1062): D95F21002140006; (D.M. 25/06/2021, n. 737): D95F21002160001. The work of the second author has been supported by the

Ministry of Education, Science and Technological Development through the project no. 451-03-68/2022-14/200156: “Innovative scientific and artistic research from the FTS domain”.

REFERENCES

[1] Petrone C, Magliulo G, Manfredi G. Seismic demand on light acceleration-sensitive nonstructural components in European reinforced concrete buildings. Earthq Eng Struct Dyn 2015;44(8):1203–1217. https://doi.org/10.1002/eqe.2508

[2] Vukobratović V, Fajfar P. A method for the direct determination of approximate floor response spectra for SDOF inelastic structures. Bull Earthq Eng 2015;13:1405–1424. https://doi.org/10.1007/s10518-014-9667-0

[3] Anajafi H, Medina RA. Lessons Learned from Evaluating the Responses of Instrumented Buildings in the United States: The Effects of Supporting Building Characteristics on Floor Response Spectra. Earthq Spectra 2019;35(1):159–191. https://doi.org/10.1193/081017EQS159M

[4] Kazantzi AK, Vamvatsikos D, Miranda E. The effect of damping on floor spectral accelerations as inferred from instrumented buildings. Bull Earthq Eng 2020;18:2149–2164. https://doi.org/10.1007/s10518-019-00781-3

[5] Chen MC, Pantoli E, Wang X, Astroza R, Ebrahimian H, Hutchinson TC, Conte JP, Restrepo JI, Marin C, Walsh KD, Bachman RE, Hoehler MS, Englekirk R, Faghihi M. Full-Scale Structural and Nonstructural Building System Performance during Earthquakes: Part I – Specimen Description, Test Protocol, and Structural Response. Earthq Spectra 2016;32(2):737–770. https://doi.org/10.1193/012414EQS016M

[6] Vukobratović V, Yeow TZ, Kusunoki K. Floor acceleration demands in three RC buildings subjected to multiple excitations during shake table tests. Bull Earthq Eng 2021;19:5495–5523. https://doi.org/10.1007/s10518-021-01181-2

[7] Petrone C, Magliulo G, Manfredi G. Floor response spectra in RC frame structures designed according to Eurocode 8. Bull Earthq Eng 2016;14:747–767. https://doi.org/10.1007/s10518-015-9846-7

[8] Anajafi H, Medina RA. Evaluation of ASCE 7 equations for designing acceleration-sensitive nonstructural components using data from instrumented buildings. Earthq Eng Struct Dyn 2018;47(4):1075–1094. https://doi.org/10.1002/eqe.3006

[9] Vukobratović V, Fajfar P. A method for the direct estimation of floor acceleration spectra for elastic and inelastic MDOF structures. Earthq Eng Struct Dyn 2016;45(15):2495–2511. https://doi.org/10.1002/eqe.2779

[10] Vukobratović V, Fajfar P. Code-oriented floor acceleration spectra for building structures. Bull Earthq Eng 2017;15:3013–3026. https://doi.org/10.1007/s10518-016-0076-4

[11] Lucchini A, Franchin P, Mollaioli F. Uniform hazard floor acceleration spectra for linear structures. Earthq Eng Struct Dyn 2017;46(7):1121–1140. https://doi.org/10.1002/eqe.2847

[12] Degli Abbati S, Cattari S, Lagomarsino S. Theoretically-based and practice-oriented formulations for the floor spectra evaluation. Earthq Struct 2018;15(5):565–581. https://doi.org/10.12989/eas.2018.15.5.565

[13] Merino RJ, Perrone D, Filiatrault A. Consistent floor response spectra for performance-based seismic design of non-structural elements. Earthq Eng Struct Dyn 2020;49(3):261–284. https://doi.org/10.1002/eqe.3236

[14] Wang T, Shang Q, Li J. Seismic force demands on acceleration-sensitive nonstructural components: a state-of-the-art review. Earthq Eng Eng Vib 2021;20:39–62. https://doi.org/10.1007/s11803-021-2004-0

[15] Çelebi M, Bongiovanni G, Şafak E, Brady AG. Seismic Response of a Large-Span Roof Diaphragm. Earthq Spectra 1989;5(2):337–350. https://doi.org/10.1193/1.1585525

[16] Tena-Colunga A. Seismic evaluation of unreinforced masonry structures with flexible diaphragms, Earthquake Spectra, 1992, 8 (2), 305-318, http://dx.doi.org/10.1193/1.1585683.

[17] Tena-Colunga, A., Abrams D. P. Response of an unreinforced masonry building during the Loma Prieta Earthquake, Structural Research Series No. 576, Department of Civil Engineering, University of Illinois at Urbana-Champaign, 1992 December.

[18] Tena-Colunga, A., Abrams D. P. Response of an instrumented masonry shear wall building with flexible diaphragms during the Loma Prieta Earthquake, Structural Research Series No. 577, Department of Civil Engineering, University of Illinois at Urbana-Champaign, 1992 December.

[19] Tena-Colunga, A., Abrams D. P. Simplified 3-D dynamic analysis of structures with flexible diaphragms, Earthquake Engineering & Structural Dynamics, 1995, 24 (2), 221-232, http://dx.doi.org/10.1002/eqe.4290240207.

[20] Tena-Colunga A, Abrams DP. Seismic Behavior of Structures with Flexible Diaphragms. J Struct Eng 1996;122(4):439–445. https://doi.org/10.1061/(ASCE)0733-9445(1996)122:4(439)

[21] Qu B, Goel RK, Chadwell CB. Evaluation of ASCE/SEI 7 Provisions for Determination of Seismic Demands on Nonstructural Components. Proceedings of the Tenth U.S. National Conference on Earthquake Engineering, Anchorage, AK, USA, 21-25 July 2014;1–11.

[22] ASCE 7-10. Minimum Design Loads for Buildings and Other Structures. Reston, VA, USA: American Society of Civil Engineers; 2010.

[23] Bernal D, Cabrera E, Rodríguez E. Diaphragm Flexibility in Floor Spectra. In: Foss G, Niezrecki C, editors. Special Topics in Structural Dynamics, Volume 6: Proceedings of the 32nd IMAC, A Conference and Exposition on Structural Dynamics, Springer International Publishing; 2014, p. 355–359. https://doi.org/10.1007/978-3-319-04729-4_31

[24] Kollerathu JA, Menon A. Role of diaphragm flexibility modelling in seismic analysis of existing masonry structures. Struct 2017;11:22–39. http://doi.org/10.1016/j.istruc.2017.04.001

[25] EN 1998-1. Eurocode 8: Design of structures for earthquake resistance - Part 1: General rules, seismic actions and rules for buildings. Brussels, Belgium: European Committee for Standardization; 2004.

[26] International Building Code. Country Club Hills, IL, USA: International Code Council; 2009.

[27] Saffarini HS, Qudaimat MM. In-Plane Floor Deformations in RC Structures. J Struct Eng 1992;118(11):3089–3102. https://doi.org/10.1061/(ASCE)0733-9445(1992)118:11(3089)

[28] Ju, S. H., Lin, M. C. (1999). Comparison of building analyses assuming rigid or flexible floors. Journal of Structural Engineering, 125(1), 25-31. https://doi.org/10.1061/(ASCE)0733-9445(1999)125:1(25)

[29] Kunnath SK, Panahshahi N, Reinhorn AM. Seismic Response of RC Buildings with Inelastic Floor Diaphragms. J Struct Eng 1991;117(4):1218–1237. https://doi.org/10.1061/(ASCE)0733-9445(1991)117:4(1218)

[30] Fleischman RB, Farrow KT, Eastman K. Seismic Performance of Perimeter Lateral-System Structures with Highly Flexible Diaphragms. Earthq Spectra 2002;18(2):251–286. https://doi.org/10.1193/1.1490547

[31] Lee HJ, Aschheim MA, Kuchma D. Interstorey drift estimates for low-rise flexible diaphragm structures. Eng Struct 2007;29(7):1375–1397. https://doi.org/10.1016/j.engstruct.2006.08.021

[32] Sadashiva VK, MacRae GA, Deam BL, Spooner MS. Quantifying the seismic response of structures with flexible diaphragms. Earthq Eng Struct Dyn 2012;41(10):1365–1389. https://doi.org/10.1002/eqe.1187

[33] Tena-Colunga A, Chinchilla-Portillo KL, Juárez-Luna G. Assessment of the diaphragm condition for floor systems used in urban buildings. Eng Struct 2015;93:70–84. https://doi.org/10.1016/j.engstruct.2015.03.025

[34] Tena-Colunga A, Liga-Paredes AE. Lateral Displacement in Walls with Openings: Importance of Floor System Stiffness. Prct Per Struct Des Const 2020;25(1):04019036. https://doi.org/10.1061/(ASCE)SC.1943-5576.0000466

[35] Tena-Colunga A. Conditions of structural irregularity. Relationships with observed earthquake damage in Mexico City in 2017. Soil Dyn Earthq Eng 2021;143:106630. https://doi.org/10.1016/j.soildyn.2021.106630

[36] Ruggieri S, Porco F, Uva G. A numerical procedure for modeling the floor deformability in seismic analysis of existing RC buildings. J Build Eng 2018;19:273–284. https://doi.org/10.1016/j.jobe.2018.05.019

[37] Ruggieri S, Porco F, Uva G. A practical approach for estimating the floor deformability in existing RC buildings: evaluation of the effects in the structural response and seismic fragility. Bull Earthq Eng 2020;18:2083–2113. https://doi.org/10.1007/s10518-019-00774-2

[38] Ruggieri S, Uva G. Accounting for the Spatial Variability of Seismic Motion in the Pushover Analysis of Regular and Irregular RC buildings in the New Italian Building Code. Bldgs 2020;10(10):177. https://doi.org/10.3390/buildings10100177

[39] Uva G, Raffaele D, Porco F, Fiore A. On the role of equivalent strut models in the seismic assessment of infilled RC buildings. Eng Struct 2012;42:83–94. https://doi.org/10.1016/j.engstruct.2012.04.005

[40] McKenna F. OpenSees: A Framework for Earthquake Engineering Simulation. Comp Sci Eng 2011;13(4):58–66. https://doi.org/10.1109/MCSE.2011.66

[41] Ibarra LF, Medina RA, Krawinkler H. Hysteretic models that incorporate strength and stiffness deterioration. Earthq Eng Struct Dyn 2005;34(12):1489–1511. https://doi.org/10.1002/eqe.495

[42] Ambraseys N, Smit P, Sigbjörnsson R, Suhadolc P, Margaris B. Internet-Site for European Strong-Motion Data; European Commission, Research-Directorate General, Environment and Climate Programme, http://isesd.hi.is/; 2002 [accessed 08 October 2021].

[43] Vukobratović V. The Influence of Nonlinear Seismic Response of Structures on the Floor Acceleration Spectra. Ph.D. Thesis, University of Ljubljana, Ljubljana, Slovenia, http://drugg.fgg.uni-lj.si/5153/; 2015 [accessed on 08 October 2021].

[44] Vukobratović V, Ruggieri S. Floor Acceleration Demands in a Twelve-Storey RC Shear Wall Building. Bldgs 2021;11(2):38. https://doi.org/10.3390/buildings11020038

[45] Petrini L, Pinho R, Calvi GM. Criteri di Progettazione Antisismica degli Edifici, 2007, IUSS Press, ISBN: 88-7358-039-4 (In Italian)

[46] Eivani H, Tena-Colunga A, Moghadam A.S. Proper configuration of stiffness and strength centers in asymmetric single-story structures with semi-flexible diaphragms. Structures, 2022, 40, 149-162. https://doi.org/10.1016/j.istruc.2022.04.022

[47] Pecce M, Ceroni F, Maddaloni G, Innuzzella V. Assessment of the in plane deformability of RC floors with traditional and innovative lightening elements in RC framed and wall structures. Bull Earthq Eng. 2017, 15:3125–3149. https://doi.org/10.1007/s10518-017-0083-0

[48] Marini A, Belleri A, Passoni C, Feroldi F, Giuriani E. In-plane capacity of existing post-WWII beam-and-clay block floor systems. Bull of Earthq Eng, 2022, 20(3), 1655-1683. https://doi.org/10.1007/s10518-021-01301-y

[49] Singh MP, Chang T-S, Suárez LE. Floor response spectrum amplification due to yielding of supporting structure. Proceedings of the Eleventh World Conference on Earthquake Engineering, Acapulco, Mexico, 23-28 June 1996; Paper No. 1444.

[50] EN 1998-3. Eurocode 8: Design of structures for earthquake resistance - Part 3: Assessment and retrofitting of buildings. Brussels, Belgium: European Committee for Standardization; 2004.

[51] Smith BS. Behavior of Square Infilled Frames. J Struct Div 1966;92(1):381–404.

[52] Panagiotakos TB, Fardis MN. Seismic response of infilled RC frames structures. Proceedings of the Eleventh World Conference on Earthquake Engineering, Acapulco, Mexico, 23-28 June 1996; Paper No. 225.

APPENDIX

Information about the applied ground motions is shown in Tables A.1, A.2 and A.3 for soils A, B and C, respectively. It should be noted that the PGV denotes peak ground velocity.

Table A.1 – Set of ground motions corresponding to the soil A

Record	Earthquake name / Earthquake date	Magnitude Mw	Epicentral distance [km]	PGA [m/s^2]	PGV [m/s]
193	Montenegro 9 Apr 1979	5.4	15	0.43	0.02
198	Montenegro 15 Apr 1979	6.9	21	2.20	0.26
198	Montenegro 15 Apr 1979	6.9	21	1.77	0.17
287	Campano Lucano 23 Nov 1980	6.9	23	1.78	0.30
287	Campano Lucano 23 Nov 1980	6.9	23	1.36	0.21
294	Campano Lucano 23 Nov 1980	6.9	26	0.90	0.16
294	Campano Lucano 23 Nov 1980	6.9	26	0.78	0.15
292	Campano Lucano 23 Nov 1980	6.9	25	0.59	0.06
292	Campano Lucano 23 Nov 1980	6.9	25	0.59	0.04
290	Campano Lucano 23 Nov 1980	6.9	32	3.17	0.55
290	Campano Lucano 23 Nov 1980	6.9	32	2.12	0.33

Table A.2 – Set of ground motions corresponding to the soil B

Record	Earthquake name / Earthquake date	Magnitude Mw	Epicentral distance [km]	PGA [m/s^2]	PGV [m/s]
413	Kalamata 13 Sep 1986	5.9	10	2.91	0.32
413	Kalamata 13 Sep 1986	5.9	10	2.11	0.33
6263	South Iceland 17 Jun 2000	6.5	7	5.02	0.50
196	Montenegro 15 Apr 1979	6.9	25	3.00	0.25
197	Montenegro 15 Apr 1979	6.9	24	2.36	0.47
196	Montenegro 15 Apr 1979	6.9	25	4.45	0.39
291	Campano Lucano 23 Nov 1980	6.9	16	1.53	0.27
199	Montenegro 15 Apr 1979	6.9	16	3.68	0.42
199	Montenegro 15 Apr 1979	6.9	16	3.56	0.52
594	Umbria Marche 26 Sep 1997	6.0	11	4.54	0.29
354	Panisler 30 Oct 1983	6.6	33	1.24	0.37

Table A.3 – Set of ground motions corresponding to the soil C

Record	Earthquake name / Earthquake date	Magnitude Mw	Epicentral distance [km]	PGA [m/s^2]	PGV [m/s]
1226	Izmit 17 Aug 1999	7.6	100	3.04	0.41
7329	Faial 9 Jul 1998	6.1	10	3.75	0.35
7329	Faial 9 Jul 1998	6.1	7	4.12	0.28
879	Dinar 1 Oct 1995	6.4	8	3.13	0.41
1257	Izmit 17 Aug 1999	7.6	20	2.90	0.52
42	Ionian 4 Nov 1973	5.8	15	2.50	0.26
1703	Duzce 1 12 Nov 1999	7.2	8	3.70	0.36
1226	Izmit 17 Aug 1999	7.6	100	3.54	0.54
1703	Duzce 1 12 Nov 1999	7.2	8	5.04	0.63
1560	Duzce 1 12 Nov 1999	7.2	39	7.85	0.65
1560	Duzce 1 12 Nov 1999	7.2	39	7.31	0.53